Inorg. Chem. **2007**, *46*, 9715–9735

Synthesis and Reactivity of $[(silox)_2Mo{=}NR]_2Hg$ (R = ^{t}Bu, ^{t}Amyl; silox = OSi^tBu_3): Unusual Thermal Stability and Ready Nucleophilic Cleavage Rationalized by Electronic Factors

Devon C. Rosenfeld,[†] Peter T. Wolczanski,*[,†] Khaldoon A. Barakat,[‡] Corneliu Buda,[‡] Thomas R. Cundari,[‡] Frank C. Schroeder,[†] and Emil B. Lobkovsky[†]

Department of Chemistry & Chemical Biology, Baker Laboratory, Cornell University, Ithaca, New York 14853, and Department of Chemistry, University of North Texas, Box 305070, Denton, Texas 76203

Received June 4, 2007

Treatment of $(DME)Cl_2Mo(=NR)_2$ (R = ^{t}Bu, (**1**-^{t}Bu), ^{t}Amyl (**1**-^{t}Amyl)) with 2 equiv of $^tBu_3SiOH$ (siloxH) and 1 equiv of HCl produced $(silox)_2Cl_2Mo{=}NR$ (R = ^{t}Bu, (**3**-^{t}Bu), ^{t}Amyl (**3**-^{t}Amyl)); subsequent reduction by Na/Hg afforded the Mo(V) chloride, $(silox)_2ClMo{=}N^tBu$ (**4**-^{t}Bu), and the Mo(IV) mercury derivatives, $[(silox)_2Mo{=}NR]_2Hg$ (R = ^{t}Bu ((**5**-^{t}Bu)$_2$Hg), ^{t}Amyl ((**5**-^{t}Amyl)$_2$Hg)). Reductions of **3**-^{t}Bu and **3**-^{t}Amyl in the presence of L (L = PMe_3, pyridine, 4-picoline) led to the isolation of adducts $(silox)_2(Me_3P)Mo{=}NR$ (R = ^{t}Bu (**6**-^{t}Bu), ^{t}Amyl (**6**-^{t}Amyl)) and $(silox)_2L_2$-$Mo{=}N^tBu$ (L = py (**7**-py), 4-pic (**7**-4-pic)). Single-crystal X-ray structural investigations of pseudo-tetrahedral **4**-^{t}Bu, Hg-capped, pseudo-trigonal planar (**5**-^{t}Bu)$_2$Hg, pseudo-tetrahedral **6**-^{t}Bu, and trigonal bipyramidal **7**-4-pic reveal that all possess a closed O–Mo–O angle when compared to the N=Mo–O angles. A molecular orbital rationale and supporting calculations suggest that this is a manifestation of the greater π-donating ability of the imido relative to that of the siloxides. While the *D*(Mo–Hg) of $[(HO)_2Mo{=}NH]_2Hg$ ((**5′**)$_2$Hg) was calculated to be 22.4 kcal/mol, (**5**-R)$_2$Hg (R =^{t}Bu, ^{t}Amyl) are remarkably stable; (**5**-^{t}Bu)$_2$Hg degraded in a first-order fashion with $\Delta G^{\ddagger}$ = 31.9(1) kcal/mol. In the presence of strong (L = PMe, pyridine, S_8) or weak (L = 2-butyne, ethylene, N_2O, 1,4,7,10-tetrathiacyclododecane, 1,4,7,10,13,16-hexathiacyclooctadecane) nucleophiles, an enhanced rate of Mo–Hg bond cleavage was noted, with some of the former group generating adducts in <5 min; the products were **6**-^{t}Bu, **7**-py, $(silox)_2(S)Mo{=}N^tBu$ (**10**-^{t}Bu), $(silox)_2Mo{=}N^tBu(C_2Me_2)$ (**8**-^{t}Bu), $(silox)_2(C_2H_4)Mo{=}N^tBu$ (**11**-^{t}Bu), $(silox)_2(O)$-$Mo{=}N^tBu$ (**9**-^{t}Bu), and a mixture of **10**-^{t}Bu and **11**-^{t}Bu, respectively. Some of these were independently prepared via substitution of **6**-^{t}Bu. According to calculations and a molecular orbital rationale, dissociation of the Mo–Hg bond in (**5**-R)$_2$Hg (R =^{t}Bu, ^{t}Amyl) is orbitally forbidden, and the addition of a nucleophile to the terminus of the Mo–Hg–Mo linkage mitigates the symmetry requirements. The mechanism of thermal degradation was studied with mixed success. NMR spectroscopy revealed imido exchange between (**5**-^{t}Bu)$_2$Hg and (**5**-^{t}Amyl)$_2$Hg during an initial induction period and a subsequent rapid exchange period that implicated free **5**-R (R = ^{t}Bu, ^{t}Amyl). Further crossover studies revealed siloxide exchange as an additional complication.

Introduction

In transition metal chemistry, unusual electronic features of either ground-state (GS) or intermediate species can play a profound role in dictating the reactivity of a complex.[1−8] Recent investigations in these laboratories have focused on oxygen atom transfer (OAT)[9−12] and substitution processes where orbital symmetry requirements governed the reactivity of $(silox)_3M + OE \rightarrow (silox)_3MO + E$ (M = V, NbL (L =

* To whom correspondence should be addressed. E-mail: ptw2@cornell.edu.
† Cornell University.
‡ University of North Texas.

(1) (a) Harvey, J. N.; Poli, R.; Smith, K. M. *Coord. Chem. Rev.* **2003**, *238*, 347−361. (b) Poli, R.; Harvey, J. N. *Chem. Soc. Rev.* **2003**, *32*, 1−8.
(2) (a) Poli, R. *J. Organomet. Chem.* **2004**, *689*, 4291−4304. (b) Poli, R. *Acc. Chem. Res.* **1997**, *30*, 1861−1866.
(3) (a) Harvey, J. N. *Struct. Bonding* **2004**, *112*, 151−183. (b) Matsunaga, N.; Koseki, S. *Rev. Comput. Chem.* **2004**, *20*, 101−152.
(4) (a) Carreon-Macedo, J. L.; Harvey, J. N. *J. Am. Chem. Soc.* **2004**, *126*, 5789−5797. (b) Carreon-Macedo, J.; Harvey, J. N.; Poli, R. *Eur. J. Inorg. Chem.* **2005**, *12*, 2999−3008.
(5) (a) Poli, R.; Cacelli, I. *Eur. J. Inorg. Chem.* **2005**, *12*, 2324−2331. (b) Petit, A.; Cacelli, I.; Poli, R. *Chem.—Eur. J.* **2006**, *12*, 813−823. (c) Smith, K. M.; Poli, R.; Harvey, J. N. *Chem.—Eur. J.* **2001**, *7*, 1679−1690.

10.1021/ic7010953 CCC: $37.00
Published on Web 10/16/2007

4-pic, PMe_3), Ta; E = PR_3, $NW(silox)_3$;[9,13] silox = $^tBu_3SiO$) and $(silox)_3M(ole) \leftrightarrow (silox)_3M + ole$ (ole = olefin).[14,15] Changes in spin state often occur in these reactions, yet it is the orbital symmetry of the states involved that appears to be reflected in unexpected kinetic effects within a group. Encouraged by these studies, a d^2 group 6 system was sought for investigations related to the d^2 group 5 compounds, and three-coordinate $(silox)_2M{=}NR$ (M = Cr, Mo, W) complexes were a logical target. The move to group 6 and the descent in symmetry from pseudo-D_{3h} to C_{2v} were expected to render ground and excited states (ES) of σ- and π-type orbital symmetry energetically closer, thereby enhancing the influence of ESs on the energies of intermediates and the rates of chemical reactions.

While $(silox)_2W{=}N^tBu$ ($S = 0$) has proven to be difficult to synthesize reproducibly, it has nonetheless been isolated, and its chemistry has been[16] and continues[17] to be explored. Likewise, $(silox)_2Cr{=}NR$ derivatives have been prepared,[18] and the weaker field of the first-row element is revealed in the $S = 1$ character of the complexes, just as $(silox)_3V$ was shown to possess a triplet GS.[9] Like $(silox)_3Nb$, whose GS is believed to be a singlet, but with an energetically nearby triplet excited state ($\Delta E(T-S) \approx +2$ kcal/mol),[9] $(silox)_2Mo{=}NR$ has proven to be quite elusive. $(silox)_3Nb$ has not been isolated, and when generated, two cyclometalated isomers (e.g., $(silox)_2HNb(\kappa\text{-O,C}-OSi^tBu_2CMe_2CH_2)$) are immediately observed instead.[9] Since cyclometallation of $(silox)_2Mo{=}NR$ may not be thermodynamically feasible, and its third row congener $(silox)_2W{=}N^tBu$ is in equilibrium with $(silox)(^tBuN{=})HW(\kappa\text{-O,C}-OSi^tBu_2CMe_2CH_2)$ ($\Delta G°(25\ °C) \approx -3$ kcal/mol),[17] attempts to synthesize $(silox)_2Mo{=}NR$ (R = ^{t}Bu, **5**-^{t}Bu; $CEtMe_2$, **5**-^{t}Amyl) were initiated using the approach employed for tungsten. This report details the chemistry of $[(silox)_2Mo{=}NR]_2Hg$ (R = ^{t}Bu, (**5**-^{t}Bu)$_2$Hg; ^{t}Amyl, (**5**-^{t}Amyl)$_2$Hg), which was prepared during the course of investigation. Its unusual electronic ground state imparts significant kinetic stability to the molecule with regard to degradation, yet permits it to serve as a source of $(silox)_2Mo{=}NR$ (R = ^{t}Bu (**5**-^{t}Bu), $CEtMe_2$ (**5**-^{t}Amyl)) in the presence of nucleophiles. A preliminary report focused on an estimate of a Mo−Mo π-bond energy (~27 kcal/mol) using spectroscopic features of (**5**-^{t}Bu)$_2$Hg.[19]

Scheme 1

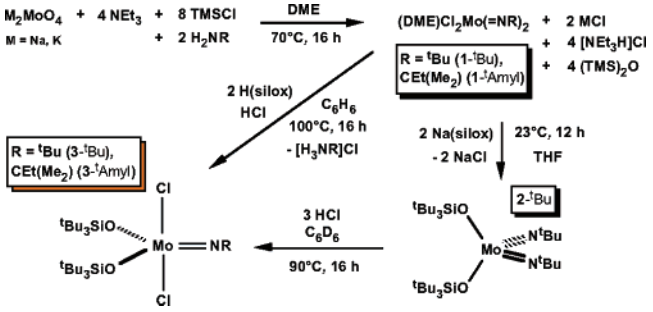

Results

Syntheses and Characterizations. 1. $(silox)_2Cl_2Mo{=}NR$ (R = ^{t}Bu (1-^{t}Bu), CEt(Me$_2$) (1-^{t}Amyl)). Using the Gibson modification[20,21] of a Schrock procedure,[22] $(DME)Cl_2Mo(=NR)_2$ (R = ^{t}Bu (**1**-^{t}Bu), ^{t}Amyl (**1**-^{t}Amyl)) was prepared from M_2MoO_4 (M = Na, K), NEt_3, TMSCl, and *tert*-butyl or *tert*-amyl amine according to Scheme 1. $(DME)Cl_2Mo(=N^tBu)_2$ was treated with 2 equiv of Na(silox) to produce colorless $(silox)_2Mo(=N^tBu)_2$ (**2**-^{t}Bu) in 54% yield, and an NMR tube-scale reaction in benzene-d_6 showed that it could be converted to $(silox)_2Cl_2Mo{=}N^tBu$ (**3**-^{t}Bu) and [^{t}BuNH$_3$]-Cl upon addition of 3 equiv of HCl. During this process, $^tBu_3SiOH$ was produced, but it readded to the molybdenum to generate the final product. Since the silanol was a proton source in its ultimate addition, a one-pot protocol to produce to $(silox)_2Cl_2Mo{=}NR$ (R = ^{t}Bu (**3**-^{t}Bu), ^{t}Amyl (**3**-^{t}Amyl)) from **1**-^{t}Bu or **1**-^{t}Amyl, 2 equiv of H(silox), and 1 equiv HCl was developed (Scheme 1), and the desired compounds were routinely produced as orange crystals in 70−80% yields. ^{1}H and $^{13}C\{^1H\}$ NMR spectral data for all new silox compounds are listed in Table 1.

2. Reductions to $(silox)_2ClMo{=}N^tBu$ (4-^{t}Bu) and $[(silox)_2Mo{=}NR]_2Hg$ (R = ^{t}Bu ((5-^{t}Bu)$_2$Hg), ^{t}Amyl

(6) (a) Schroder, D.; Shaik, S.; Schwarz, H. *Acc. Chem. Res.* **2000**, *33*, 139−145. (b) de Visser, S. P.; Shaik, S.; Sharma, P. K.; Kumar, D.; Thiel, W. *J. Am. Chem. Soc.* **2003**, *125*, 15779−15788. (c) Kumar, D.; de Visser, S. P.; Shaik, S. *J. Am. Chem. Soc.* **2003**, *125*, 13024−13025. (d) Sharma, P. K.; de Visser, S. P.; Shaik, S. *J. Am. Chem. Soc.* **2003**, *125*, 8689−8699.

(7) (a) Hess, J. S.; Leelasubcharoen, S.; Rhenigold, A. L.; Doren, D. J.; Theopold, K. H. *J. Am. Chem. Soc.* **2002**, *124*, 2454−2455. (b) Detrich, J. L.; Reinaud, O. M.; Rheingold, A. L.; Theopold, K. H. *J. Am. Chem. Soc.* **1995**, *117*, 11745−11748.

(8) De Angelis, F.; Jin, N.; Car, R.; Groves, J. T. *Inorg. Chem.* **2006**, *45*, 4268−4276.

(9) (a) Veige, A. S.; Slaughter, L. M.; Lobkovsky, E. B.; Wolczanski, P. T.; Matsunaga, N.; Decker, S. A.; Cundari, T. R. *Inorg. Chem.* **2003**, *42*, 6204−6224. (b) Veige, A. S.; Slaughter, L. M.; Wolczanski, P. T.; Matsunaga, N.; Decker, S. A.; Cundari, T. R. *J. Am. Chem. Soc.* **2001**, *123*, 6419−6420.

(10) Rosenfeld, D. C.; Kuiper, D. S.; Lobkovsky, E. B.; Wolczanski, P. T. *Polyhedron* **2006**, *25*, 251−258.

(11) Veige, A. S.; Kleckley, T. S.; Chamberlin, R. L. M.; Neithamer, D. R.; Lee, C. E.; Wolczanski, P. T.; Lobkovsky, E. B.; Glassey, W. V. *J. Organomet. Chem.* **1999**, *591*, 194−203.

(12) Bonanno, J. B.; Henry, T. P.; Neithamer, D. R.; Wolczanski, P. T.; Lobkovsky, E. B. *J. Am. Chem. Soc.* **1996**, *118*, 5132−5133.

(13) Hirsekorn, K. F.; Veige, A. S.; Wolczanski, P. T. *J. Am. Chem. Soc.* **2006**, *128*, 2192−2193.

(14) (a) Hirsekorn, K. F., Ph.D. Thesis, Cornell University, Ithaca, NY, 2006. (b) Hirsekorn, K. F.; Hulley, E. B.; Wolczanski, P. T.; Cundari, T. R. Unpublished work.

(15) Hirsekorn, K. F.; Veige, A. S.; Marshak, M. P.; Koldobskaya, Y.; Wolczanski, P. T.; Cundari, T. R.; Lobkovsky, E. B. *J. Am. Chem. Soc.* **2005**, *127*, 4809−4830.

(16) Eppley, D. F.; Wolczanski, P. T.; Van Duyne, G. D. *Angew. Chem., Int. Ed. Engl.* **1991**, *30*, 584−585.

(17) Marshak, M. P.; Rosenfeld, D. C.; Eppley, D. F.; Wolczanski, P. T.; Cundari, T. R.; Lobkovsky, E. B. Unpublished work.

(18) Sydora, O. L.; Kuiper, D. S.; Wolczanski, P. T.; Lobkovsky, E. B.; Dinescu, A.; Cundari, T. R. *Inorg. Chem.* **2006**, *45*, 2008−2021.

(19) Rosenfeld, D. C.; Wolczanski, P. T.; Barakat, K. A.; Buda, C.; Cundari, T. R. *J. Am. Chem. Soc.* **2005**, *127*, 8262−8263. Details of the calculations for $(HO)_2Mo{=}NH$ (**5′**) and $[(HO)_2Mo{=}NH]_2Hg$ (**5′**$_2$-Hg) and the dissociation of the latter into $(HO)_2Mo{=}NH$ (**5′**) and $(HO)_2HgMo{=}NH$ (**5′**-Hg) are given in the Supporting Information for this communication.

(20) Dyer, P. W.; Gibson, V. C.; Howard, J. A. K.; Whittle, B.; Wilson, C. *J. Chem. Soc., Chem. Commun.* **1992**, 1666−1668.

(21) Barrie, P.; Coffey, T. A.; Forster, G. D.; Hogarth, G. *J. Chem. Soc., Dalton Trans.* **1999**, 4519−4528.

(22) Fox, H. H.; Yap, K. B.; Robbins, J.; Cai, S.; Schrock, R. R. *Inorg. Chem.* **1992**, *31*, 2287−2289.

Table 1. ^{1}H and ^{13}C{^{1}H} NMR Spectral Assignments on (silox)$_2$Mo═NR Derivatives in C_6D_6

	^{1}H NMR (δ m, J(Hz), asmt)[a]					^{13}C{^{1}H} (δ,(asmt)[b]		
	Si^{t}Bu	NR	other	Si*C*	NC	$(CH_3)_3$	NR	other
(silox)$_2$Mo(N^{t}Bu)$_2$ (**2**-^{t}Bu)	1.26	1.39		24.22	69.83	30.51	32.52	
(silox)$_2$Cl$_2$MoN^{t}Bu (**3**-^{t}Bu)	1.35	1.26		25.37	82.64	30.65	29.77	
(silox)$_2$Cl$_2$MoNC(Me)$_2$Et (**3**-^{t}Amyl)	1.37	0.95, t, 7, Me 1.30 Me$_2$ 1.61, q, 7, CH_2		25.35	86.49	30.65	9.45, CH_3 26.20, $(CH_3)_2$ 36.12, CH_2	
(silox)$_2$ClMoN^{t}Bu (**4**-^{t}Bu)	2.6 $\nu_{1/2}$ = 72	−32.6 $\nu_{1/2}$ = 76						
[(silox)$_2$MoN^{t}Bu]$_2$Hg (**5**-^{t}Bu)$_2$Hg	1.96 $\nu_{1/2}$ = 18	−1.15 $\nu_{1/2}$ = 24						
[(silox)$_2$MoNC(Me)$_2$Et]$_2$Hg (**5**-^{t}Amyl)$_2$Hg	1.96 $\nu_{1/2}$ = 18	−0.87 Me$_2$ $\nu_{1/2}$ = 31 −0.17, CH_2 $\nu_{1/2}$ = 32 0.22, CH_3 $\nu_{1/2}$ = 28						
(silox)$_2$(Me$_3$P)MoN^{t}Bu (**6**-^{t}Bu)[d]	1.16	1.92	1.06, d,[c] 9, PCH_3	23.39	75.06	30.85	33.06	24.10, d,[c] 28, PC
(silox)$_2$(Me$_3$P)MoN^{t}Amyl (**6**-^{t}Amyl)[e]	1.17	1.18, Me_2, 2.24, q, 7, CH_2	1.07, d,[c] 10, PMe_3	23.42	78.47	30.87	10.43, CH_3, 30.67, $(CH_3)_2$ 37.97, CH_2	24.26, d,[c] 28, PC
(silox)$_2$(py)$_2$MoN^{t}Bu (**7**- py)	1.02	1.85	6.22, t, 7, *p*[f] 6.89, *m*[f] 8.62, *o*[f]	23.46	75.81	30.77	32.62	119.93[f] 123.48[f] 131.66, 4-C 146.89[f,g] 148.89[f,g]
(silox)$_2$(4-pic)$_2$MoN^{t}Bu (**7**-4-pic)	1.05	1.95	2.05, 4-Me 6.50, *m* 8.56, *o*	23.49	75.52	30.82	32.70	19.41, 4-CH_3 121.52[f] 123.94[f] 143.24, 4-C 147.74[f,g]
(silox)$_2$(MeCCMe)MoN^{t}Bu (**8**-^{t}Bu)	1.29	1.13	2.48, CH_3	23.88	71.67	30.59	31.55	17.92, CCH_3 179.15, CCH_3
(silox)$_2$(O)MoN^{t}Bu (**9**-tBu)	1.21	1.43		24.03	72.80	30.09	30.49	
(silox)$_2$(S)MoN^{t}Bu (**10**-tBu)	1.21	1.50		24.43	74.47	30.19	29.90	
(silox)$_2$(C_2H_4)MoN^{t}Bu (**11**-^{t}Bu)	1.23	1.19	1.83, d, 6, C*H*H 2.79, d, 6, CH*H*	23.47	74.01	30.40	30.32	52.06, C═C

[a] Referenced to C_6D_5H at δ 7.15. Linewidths at half-height ($\nu_{1/2}$) are in Hz. [b] Referenced to C_6D_5H at δ 128.00. [c] J_{PC}. [d] ^{31}P{^{1}H} NMR δ 62.84. [e] ^{31}P{^{1}H} NMR δ 63.67, t for CH_3 group could not be assigned. [f] Broad resonances caused by slow ring rotation, T_c (^{1}H) ≈ 25 °C. [g] Assigned as 2-C, 6-C, or both.

((5-^{t}Amyl)$_2$Hg)). If the molybdenum system behaved like its tungsten analogue,[16,17] Mg° reduction of the dichlorides (silox)$_2$Cl$_2$Mo═NR (R = ^{t}Bu (**3**-^{t}Bu), ^{t}Amyl (**3**-^{t}Amyl)) would have led to (silox)$_2$Mo═NR (R = ^{t}Bu (**5**-^{t}Bu), ^{t}Amyl (**5**-^{t}Amyl)), but this was not the case, despite a variety of conditions and solvents (Et_2O, THF, DME, and benzene). ^{1}H NMR analysis of the reaction mixtures revealed at least three siloxide-containing products: two were diamagnetic, and the other was paramagnetic. Little progress was achieved by changing reducing agents: Zn°, Sn°, sodium naphthalide, potassium on graphite (K/C_8), etc.

Initial success was achieved with a slight excess of 2 equiv of Na/Hg (0.95%) and (silox)$_2$Cl$_2$Mo═N^{t}Bu (**3**-^{t}Bu) in benzene for 12 h, which afforded purple (silox)$_2$ClMo═N^{t}Bu (**4**-^{t}Bu) in low yield (15%). It was subsequently identified in the NMR spectroscopic assay of the Mg° reductions, and its synthesis was optimized to 58% using a slight excess of 1 equiv of Na/Hg with **3**-^{t}Bu in Et_2O for 12 h (Scheme 2). The ^{1}H NMR spectrum of **4**-^{t}Bu exhibited broad resonances

Scheme 2

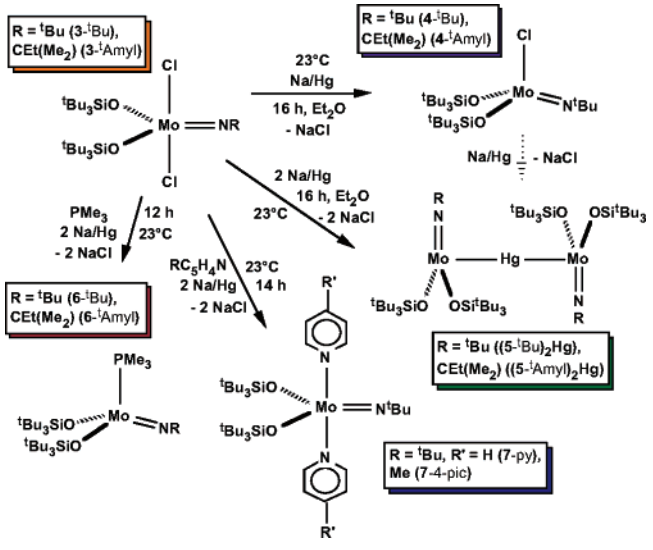

at δ 2.62 ($\nu_{1/2}$ = 72 Hz, 54 H, C(CH$_3$)$_3$) and −3.26 ($\nu_{1/2}$ = 76 Hz, 9 H, NC(CH$_3$)$_3$), and an Evans' measurement[23] revealed a solution μ_{eff} of 1.65 μ_B at 23 °C consistent with a d^1 Mo(V) complex.

When Et$_2$O was used as the solvent in Na/Hg (>2 equiv, 16 h) reductions of (silox)$_2$Cl$_2$Mo═N^{t}Bu (**3**-^{t}Bu), an olive green solid was produced. The material was paramagnetic, and its ^{1}H NMR spectrum (Table 1) consisted of broad singlets at δ 1.96 ($\nu_{1/2}$ = 18 Hz, 54 H, C(CH$_3$)$_3$) and −1.15 ($\nu_{1/2}$ = 24 Hz, 9 H, NC(CH$_3$)$_3$). Since it was plausible that (silox)$_2$Mo═N^{t}Bu (**5**-^{t}Bu) was paramagnetic, an Evans' method[23] determination of μ_{eff} was conducted, but the value of 1.15 μ_B obtained seemed low for a simple Mo(IV) paramagnet. A single-crystal X-ray structure determination of the complex identified it as [(silox)$_2$Mo═N^{t}Bu]$_2$Hg ((**5**-^{t}Bu)$_2$Hg),[19] and the ^{t}Amyl-derivative, [(silox)$_2$Mo═N^{t}Amyl]$_2$Hg ((**5**-^{t}Amyl)$_2$Hg) was subsequently produced in a similar vein. The Hg-bridged[24,25] trinclear (**5**-^{t}Bu)$_2$Hg was optimized at 58% yield, while the corresponding (**5**-^{t}Amyl)$_2$Hg species was only made a few times for crossover experiments (vide infra): 39% was the best yield obtained. From ^{1}H NMR analysis of the reductions, it is likely that (silox)$_2$ClMo═NR (R = ^{t}Bu (**4**-^{t}Bu), ^{t}Amyl (**4**-^{t}Amyl)) are intermediates in the formation of the Hg complexes.

3. Magnetism of [(silox)$_2$Mo═N^{t}Bu]$_2$Hg ((5-^{t}Bu)$_2$Hg). Magnetic studies on [(silox)$_2$Mo═N^{t}Bu]$_2$Hg ((**5**-^{t}Bu)$_2$Hg) were performed by Prof. Karsten Meyer (UCSD) using a SQUID magnetometer from 0−300 K at 1 T. The χ_M of (**5**-^{t}Bu)$_2$Hg versus T(K) plot shown in Figure 1 indicates that temperature-independent paramagnetism (TIP) is the major and perhaps only significant contributor to the paramagnetism of the complex. A second plot of μ_{eff} of (**5**-^{t}Bu)$_2$Hg versus T(K) indicates an S = 0 ground state at 0 K that has considerable triplet character at 300 K, and the μ_{eff} of 1.65 μ_B at 300 K is slightly greater than the 1.15 μ_B obtained from solution measurements. The TIP is derived from the small HOMO/LUMO gap in (**5**-^{t}Bu)$_2$Hg, whereby the π^b HOMO and π^* LUMO are close in energy because of the separation of the Mo centers by the mercury atom. An analysis of this situation provided crucial evidence that enabled the dimolybdenum π-bond to be estimated at ∼27 kcal/mol, as previously described.[19]

4. Reductions to (silox)$_2$(Me$_3$P)Mo═NR (R = ^{t}Bu (6-^{t}Bu), ^{t}Amyl (6-^{t}Amyl)) and (silox)$_2$L$_2$Mo═N^{t}Bu (L = py (7-py), 4-pic (7-4-pic)). Other derivatives of (silox)$_2$Mo═NR (R = ^{t}Bu (**5**-^{t}Bu), ^{t}Amyl (**5**-^{t}Amyl)) were prepared via Na/Hg reductions of the dichlorides (silox)$_2$Cl$_2$Mo═NR (R = ^{t}Bu (**3**-^{t}Bu), ^{t}Amyl (**3**-^{t}Amyl)). In neat PMe$_3$, the diamagnetic, maroon phosphine adducts (silox)$_2$(Me$_3$P)Mo═NR (R = ^{t}Bu (**6**-^{t}Bu), ^{t}Amyl (**6**-^{t}Amyl)) were prepared in 76 and 59% yields, respectively. When smaller heterocyclic solvents were used as the reduction medium, *bis*-adducts formed.

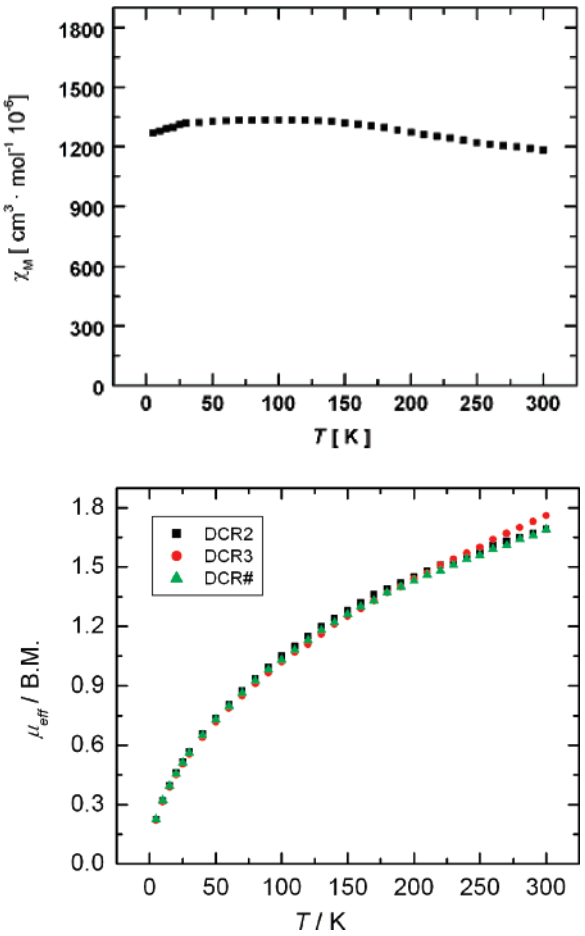

Figure 1. χ_M (cm^3 mol^{-1} (×10^{-6})) vs T (K) plot (top) for [(silox)$_2$Mo═N^{t}Bu]$_2$Hg ((**5**-^{t}Bu)$_2$Hg) measured at 1 T. A μ_{eff} (μ_B = B.M.) vs T(K) plot (bottom) for three samples of (**5**-^{t}Bu)$_2$Hg measured at 1 T.

Reduction of **3**-^{t}Bu in pyridine (py) or 4-picoline (4-pic) with a slight excess of 2 equiv of Na/Hg provided the diamagnetic, blue-purple (silox)$_2$L$_2$Mo═N^{t}Bu (L = py (**7**-py), 4-pic (**7**-4-pic)) derivatives in 60 and 58% yields, respectively. In the case of **7**-py, K/C$_8$ was also used as a reducing agent with modest success (47% yield). ^{1}H and ^{13}C{^{1}H} NMR spectroscopic data for the compounds are compiled in Table 1. Resonances for the protons in the 2, 3, 5 and 6 positions on the bound pyridines and 4-picolines were broad, prompting a variable-temperature study. Variable-temperature ^{1}H NMR spectra from 90 to −50 °C collected on **7**-py in toluene-d_8 revealed coalescence of the pyridine resonances at 25 °C. The observation was interpreted as reflecting the rotation of the pyridine and 4-picoline rings about the N−Mo−N axis: $\Delta G^{\ddagger}$ = 14.1(1) kcal/mol and T_c = 25(2)° C (500 MHz). Given the fluxional nature of many 5-coordinate molecules, an axial−equatorial interchange of silox and pyridine (4-picoline) units coupled with rotation of the pyridines (picolines) in the equatorial position affords an alternative explanation.

Single-Crystal X-ray Structure Determinations. 1. (silox)$_2$ClMo═N^{t}Bu (4-^{t}Bu). Crystallographic data for (silox)$_2$ClMo═N^{t}Bu (**4**-^{t}Bu) is listed in Table 2, and pertinent interatomic distances and angles are given in Table 3. Monochloride **4**-^{t}Bu is pseudo-tetrahedral, as illustrated by Figure 2, with slightly shorter molybdenum−oxygen dis-

(23) (a) Evans, D. F. *J. Chem. Soc.* **1959**, 2003−2005. (b) Orrell, K. G.; Sik, V. *Anal. Chem.* **1980**, *52*, 567−569. (c) Schubert, E. M. *J. Chem. Educ.* **1992**, *69*, 62.
(24) Green, M. L. H.; Konidaris, P. C.; Mountford, P. *J. Chem. Soc., Dalton Trans.* **1994**, 2851−2859.
(25) Williams, D. S.; Schofield, M. H.; Schrock, R. R.; Davis, W. M.; Anhaus, J. T. *J. Am. Chem. Soc.* **1991**, *113*, 5480−5481.

Table 2. Crystallographic Data for (silox)$_2$ClMo=N^{t}Bu (**4**-^{t}Bu), [(silox)$_2$Mo=N^{t}Bu]$_2$Hg ((**5**-^{t}Bu)$_2$Hg), (silox)$_2$(Me$_3$P)Mo=N^{t}Bu (**6**-^{t}Bu), and (silox)$_2$(4-pic)$_2$Mo=N^{t}Bu (**7**-4-pic)

	4-^{t}Bu	(**5**-^{t}Bu)$_2$Hg	**6**-^{t}Bu	**7**-4−pic
formula	$C_{28}H_{63}O_2NSi_2ClMo$	$C_{28}H_{63}O_2Si_2NMoHg_{0.5}$	$C_{31}H_{72}O_2Si_2NPMo$	$C_{40}H_{77}O_3N_3Si_2Mo$
fw	633.36	698.21	673.99	784.17
space group	$P\bar{1}$	$P2_1/n$	$P2_1/c$	$P2_1/n$
Z	2	4	4	4
a, Å	8.6651(7)	13.922(3)	9.3696(5)	14.427(3)
b, Å	12,4896(9)	15.656(2)	17.9130(10)	17.843(2)
c, Å	17.2926(13)	16.346(3)	23.8114(13)	17.766(3)
α, deg	98.231(2)	90	90	90
β, deg	99.950(2)	93.357(5)	99.4590(10)	90.053(8)
γ, deg	97.400(2)	90	90	90
V, Å^3	1801.6(2)	3556.8(14)	3942.1(4)	4573.3(14)
ρ_{calcd}, g cm^{-3}	1.168	1.304	1.136	1.139
μ, mm^{-1}	0.527	2.605	0.458	0.372
temp, K	173(2)	173(2)	173(2)	173(2)
λ, Å	0.71073	0.71073	0.71073	0.71073
R indices	$R_1 = 0.0388$	$R_1 = 0.0380$	$R_1 = 0.0531$	$R_1 = 0.1001$
$[I > 2\sigma(I)]^{b,c}$	$R_2 = 0.0931$	$R_2 = 0.0805$	$R_2 = 0.1237$	$R_2 = 0.2078$
R indices	$R_1 = 0.0526$	$R_1 = 0.0680$	$R_1 = 0.0685$	$R_1 = 0.1150$
(all data)^{b,c}	$R_2 = 0.0993$	$R_2 = 0.0887$	$R_2 = 0.1307$	$R_2 = 0.2147$
GOF^d	1.020	1.040	1.098	1.208

[a] The asymmetric unit is half of the formula unit. [b] $R_1 = \sum||F_o| - |F_c||/\sum|F_o|$. [c] $R_2 = [\sum w(|F_o| - |F_c|)^2/\sum wF_o^2]^{1/2}$. [d] GOF (all data) = $[\sum w(|F_o| - |F_c|)^2/(n - p)]^{1/2}$, n = number of independent reflections, p = number of parameters.

tances (1.8669(14) and 1.8894(14) Å) than the Mo(IV) derivatives, and a very short Mo=N bond (1.7057(18) Å).[26,27] Despite the steric bulk of the silox groups, the O1−Mo1−O2 angle of 111.32(7)° is *less* than the N=Mo−O1 and −O2 angles of 115.90(8) and 115.03(9)°, respectively. Significant distortions are evident in the remaining core angles, with the Cl−Mo−O1 angle of 98.72° being considerably smaller than the Cl−Mo=N angle of 102.45(8)° and the Cl−Mo−O2 angle of 111.75(6)°. The C1−N=Mo angle barely deviates from linearity at 177.57(19)°.

2. [(silox)$_2$Mo=N^{t}Bu]$_2$Hg ((5-^{t}Bu)$_2$Hg). Crystallographic data and interatomic distances and angles for [(silox)$_2$Mo=N^{t}Bu]$_2$Hg ((**5**-^{t}Bu)$_2$Hg) are given in Tables 2 and 3, respectively, while views of the C_{2h} molecule are displayed in Figure 3. Two pseudotrigonal planar (silox)$_2$Mo=N^{t}Bu units are linearly bridged by a Hg atom, and the d(Mo−Hg) of 2.6810(5) Å is close to the sum of covalent radii (r_{cov}(Mo) = 1.30 Å; r_{cov}(Hg) = 1.44 Å; $\sum r_{cov}$ = 2.74 Å). This distance and the crystallographically imposed Mo−Hg−Mo angle of 180° are comparable to the only other non-carbonyl Hg-bridged molybdenum compound, [Cp*(C$_2$H$_4$)$_2$Mo=N^{t}Bu]$_2$Hg (d(Mo−Hg) = 2.730 Å; Mo−Hg−Mo = 175.8°).[24] Two-coordinate mercury typically possesses a linear arrangment, as also found in [CpMo(CO)$_3$]$_2$Hg[28] and [(2,6-^{i}Pr$_2$C$_6$H$_3$N)$_3$Re]$_2$Hg.[25] There is a modest cant of the imido group toward the mercury, as the N=Mo−Hg angle of 84.51(8)° indicates in comparison to the O1−Mo−Hg and O2−Hg−Mo angles of 103.37(7) and 105.42(7)°, respectively.

The 1.718(3) Å molybdenum−nitrogen distance is typical for a Mo(IV) imido ligand,[26,27] and the C1−N=Mo angle is 176.2(2)° in agreement with the strong N → Mo π-donation. The d(Mo1−O1) of 1.894(2) Å and d(Mo1−O2) of 1.905(2) Å are also fairly short but are slightly longer than those of the Mo(V) monochloride, (silox)$_2$ClMo=N^{t}Bu (**4**-^{t}Bu). The pseudotrigonal planar geometry at molybdenum is revealed by the angles N=Mo1−O1 = 119.91(11)°, N=Mo1−O2 = 121.33(11)°, and O1−Mo1−O2 = 113.60(9)°. The closing of the O1−Mo−O2 angle from 120° is in complete contrast to the trigonal planar angles of (silox)$_2$W=N^{t}Bu, which are O−W−O = 127.4(6)° and O−W−N = 115.7(8)and 116.8(8)°,[19] but are in line with the related angle in **4**-^{t}Bu. Steric effects were argued to be the origin of the wider angle in the W case, but there may be an electronic origin to the distortion in [(silox)$_2$Mo=N^{t}Bu]$_2$Hg ((**5**-^{t}Bu)$_2$Hg).

3. (silox)$_2$(Me$_3$P)Mo=N^{t}Bu (6-^{t}Bu). Crystallographic and metric parameters are available in Tables 2 and 3, respectively, while a molecular view of pseudotetrahedral (silox)$_2$(Me$_3$P)Mo=N^{t}Bu (**6**-^{t}Bu) is given in Figure 4. The molybdenum phosphorus distance, d(Mo−P) = 2.3202(8) Å, compares favorably with literature values of related compounds.[26] The molybdenum imido bond is too long at 1.833(3) Å to be believable in view of its accompanying N1−C1 distance of 1.369(4) Å, which is roughly 0.08 Å shorter than other imido linkages. The origin to the failure of the model for this connectivity is not clear, but a subtraction of 0.08 Å to the stated d(Mo=N) would leave a molybdenum−nitrogen bond distance of 1.75 Å, which is certainly a more apt estimate of the true length,[26,27] especially since the linkage is close to linear (174.8(2)°). The Mo−O distances of 1.963(2) and 1.9354(18) Å are also somewhat long but appear to accurately reflect a more electron-rich metal center because their corresponding d(Si−O) values are normal.

Once again, the O1−Mo−O2 angle of 108.04(8)° is less than the N=Mo1−O1 and N=Mo−O2 angles of 125.85(10) and 116.15(10)°, respectively, which are considerably different. In addition, the phosphorus is canted away from O2, with O1−Mo−P = 94.05(7)° and N=Mo−P = 92.15(7)° much smaller than O2−Mo−P = 117.43(7)°. Sterically, one would predict the PMe$_3$ to lean away from the bulky silox groups and toward the slightly smaller *tert*-butyl imido

(26) Wigley, D. E. *Prog. Inorg. Chem.* **1994**, *42*, 239−482.
(27) Nugent, W. A.; Mayer, J. M. *Metal−Ligand Multiple Bonds*; Wiley-Interscience: New York, 1988.
(28) Mickiewicz, M. M.; Raston, C. L.; White, A. H.; Wild, S. A. *Aust. J. Chem.* **1977**, *30*, 1685−1691.

Table 3. Selected Interatomic Distances (Å) and Angles (deg) for $(silox)_2ClMo{=}N^tBu$ (**4**-^{t}Bu), $[(silox)_2Mo{=}N^tBu]_2Hg$ ((**5**-^{t}Bu)$_2$Hg), $(silox)_2(Me_3P)Mo{=}N^tBu$ (**6**-^{t}Bu), and $(silox)_2(4\text{-pic})_2Mo{=}N^tBu$ (**7**-4-pic) and Computed Values for $[(HO)_2Mo{=}NH]_2Hg$ (**5′**-Hg), $(HO)_2HgMo{=}NH$ (**5′**-Hg), and $(HO)_2Mo{=}NH$ (**5′**)

	(**5**-^{t}Bu)$_2$Hg[a,b]	**5′**-Hg	**5′**-Hg	**5′**	**4**-^{t}Bu[c,d]	**6**-^{t}Bu[e,f]	**7**-4−pic[g,h]
Mo−O1	1.894(2)	1.92	1.93	1.93	1.8894(14)	1.963(2)	2.003(4)
Mo−O2	1.905(2)	1.93	1.93	1.93	1.8669(14)	1.9354(18)	2.002(4)
Mo=N	1.718(3)	1.73	1.74	1.74	1.7057(18)	1.833(3)[f]	1.725(5)
Mo−X/L	2.6810(5)	2.75	3.08		2.2729(8)	2.3202(8)	2.147(5)
							2.131(5)
O1−Si1	1.635(2)				1.6464(15)	1.631(2)	1.618(4)
O2−Si2	1.636(2)				1.6534(15)	1.6275(19)	1.631(4)
N−C1	1.451(4)				1.454(3)	1.369(4)[f]	1.469(9)
$(P-C)_{av}$						1.832(4)	
$(Si-C)_{av}$	1.918(5)				1.922(5)	1.931(4)	1.939(8)
$(C-C)_{sil,av}$	1.54(5)[b]				1.537(8)	1.540(6)	1.536(17)
$(C-C)_{im,av}$	1.523(13)				1.51(6)[d]	1.523(6)	1.523(17)
$(N-C)_{pic,av}$							1.359(7)
$(C-C)_{pic,rg,av}$							1.378(10)
$(C-CH_3)_{av}$							1.507(11)
O1−Mo−O2	113.60(9)	115	117	117	111.32(7)	108.04(8)	115.70(18)
O1−Mo=N	119.91(11)	118	119	120	115.90(8)	125.85(10)	121.5(2)
O2−Mo=N	121.33(11)	121	122	123	115.03(9)	116.15(10)	122.8(2)
O1−Mo−X/L	103.37(7)	96	92		98.72(6)	94.05(7)	86.09(18)
							84.97(19)
O2−Mo−X/L	105.42(7)	107	93		111.75(6)	117.43(7)	87.11(18)
							85.85(18)
N=Mo−X/L	84.51(8)	90	97		102.45(8)	92.15(7)	98.3(2)
							96.8(2)
N2−Mo−N3							164.9(2)
Mo−O1−Si1	168.67(15)				167.68(10)	149.85(15)	159.1(3)
Mo−O2−Si2	165.74(14)				174.35(10)	164.69(13)	157.7(3)
Mo=N−C1	176.2(2)				177.57(19)	174.8(2)	177.4(5)
$(N-C1-C)_{im,}$av	108.20(17)				107.8(30)[d]	107.7(17)	108.6(8)
Mo−Hg−Mo	180						
Mo−P−C5						119.43(14)	
Mo−P−C6						109.13(14)	
Mo−P−C7						121.66(16)	
$(O-Si-C)_{av}$	106.1(6)				105.6(12)	106.8(15)	108.2(21)
$(C-Si-C)_{av}$	112.6(3)				113.1(3)	112.0(4)	110.7(7)
$(Si-C-C)_{av}$	111.4(26)[b]				111.5(12)	111.6(17)	111.8(19)
$(C-C-C)_{sil,av}$	109(11)[b]				107.4(16)	107.3(11)	107.0(12)
$(C-C-C)_{iim,av}$	110.7(9)				111.0(34)[d]	111.2(2)	110.3(7)
$(C-P-C)_{av}$						101.3(19)	
$(C-N-C)_{py,av}$							115.2(4)
$(N-C-C)_{py,av}$							123.6(11)
$(C-C-C)_{py,av}$							120.3(24)

[a] X/L = Hg. [b] Reflects severe disorder problems in silox ^{t}Bu groups. [c] X/L = Cl. [d] Reflects imido ^{t}Bu group disorder. [e] X/L = P. [f] Imido nitrogen position is questionable; assuming d(N1−C1) is 1.45 Å, then *d*(Mo=N) is ∼ 1.75 Å. [g] X/L are the two pyridine nitrogens, N2 and N3. [h] Poor data quality may be caused by twinning.

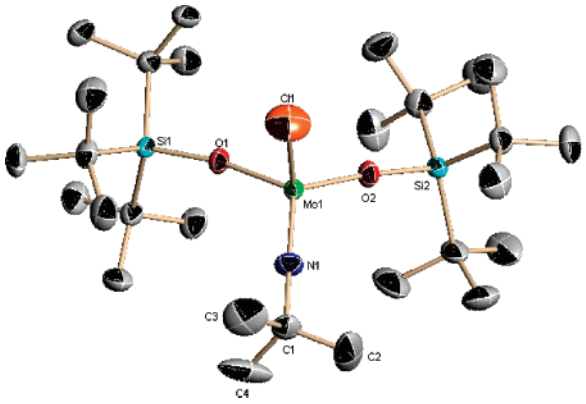

Figure 2. Molecular view of $(silox)_2ClMo{=}N^tBu$ (**4**-^{t}Bu).

ligand, so it is likely the distortion is electronic in nature. Another feature that manifests electronic effects is the cant of the entire PMe_3 unit; one Mo−P−C angle is significantly less than the other two (109.13(14) vs 119.43(14) and 121.66(16)°), and this methyl is oriented opposite the imide. Normal C−P−C angles are observed; hence the lean of the PMe_3 group has the consequence of maximizing backbonding to a 3d/σ^* phosphorus orbital that is oriented perpendicular to the imide.

4. $(silox)_2(4\text{-pic})_2Mo{=}N^tBu$ (7-4-pic). Tables 2 and 3 also contain the crystallographic and metric data pertaining to $(silox)_2(4\text{-pic})_2Mo{=}N^tBu$ (**7**-4-pic), whose pseudotrigonal bipyramidal (tbp) C_{2v} structure is illustrated by the two views in Figure 5. The 4-picolines occupy axial sites, and the two silox groups and the imido occupy equatorial positions (N=Mo−O1 = 121.5(2)°, N=Mo−O2 = 122.8(2)°, O1−Mo−O2 = 115.70(18)°, Σ(eq angles) = 360.0°), in which the oxygens are yet again pinched together in apparent contradiction to steric influences. However, the ^{t}Bu$_3$Si groups are canted away from the N_3Mo plane, with Mo−O1−Si1 and Mo−O2−Si2 angles of 159.1(3) and 157.7(3)°, respectively. The 4-picoline ligands are essentially in the N_3Mo plane and are tipped toward the opening between the silox groups, with N2−Mo−N3 = 164.9(2)°, N=Mo1−N2 =

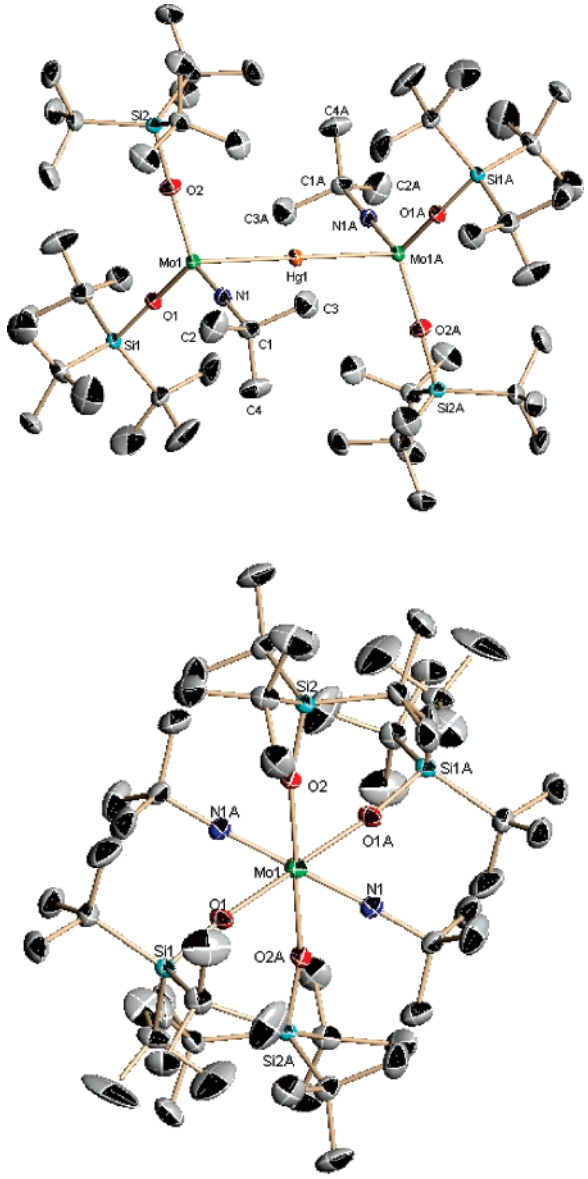

Figure 3. Molecular views (side and down the Mo_2Hg axis) of $[(silox)_2Mo{=}N^tBu]_2Hg$ ((**5**-^{t}Bu)$_2$Hg).

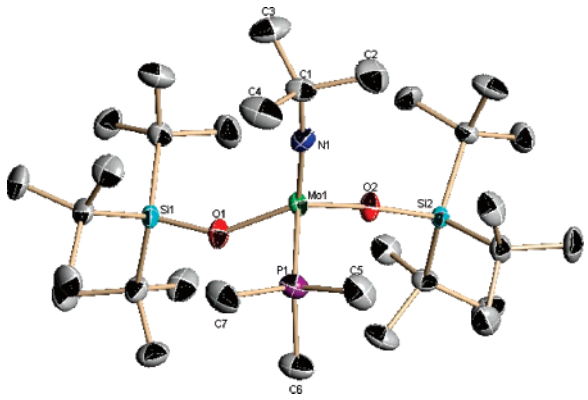

Figure 4. Molecular view of tetrahedral $(silox)_2(Me_3P)Mo{=}N^tBu$ (**6**-^{t}Bu).

98.3(2)°, N═Mo1−N3 = 96.8(2)°, O1−Mo1−N2 = 86.09-(18)°, O2−Mo1−N2 = 87.11(18)°, O1−Mo1−N3 = 84.97-(19)° and O2−Mo1−N3 = 85.85(18)°. From the figure,

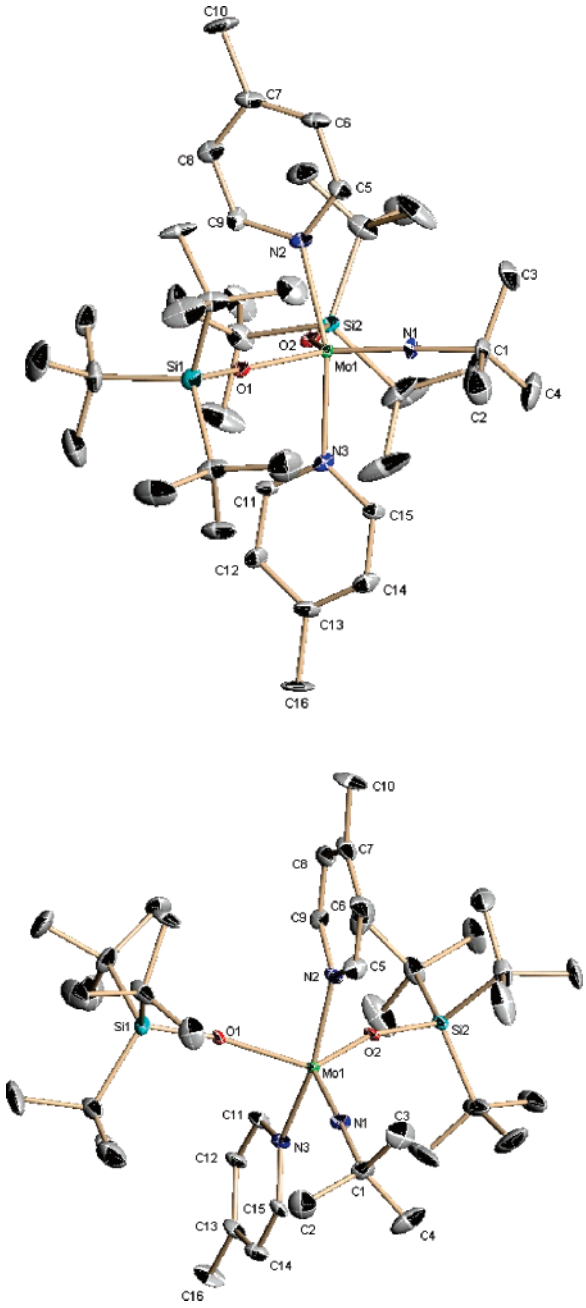

Figure 5. Molecular views of pseudo-tbp $(silox)_2(4\text{-pic})_2Mo{=}N^tBu$ (**7**-4-pic).

rotation of the picoline units, estimated to be associated with a ∼14 kcal/mol barrier based on the aforementioned variable-temperature ^{1}H NMR result, must occur with some difficulty as the picolines must slide out of the gap between silox groups to rotate. As stated above, a Berry pseudorotation event may aid the process. The *d*(Mo−O) of 2.003(4) and 2.002(4) Å are longer than in the 4-coordinate species; the *d*(Mo═N) of the nearly linear imido group (177.4(5)°) is 1.725(5) Å is marginally longer[26,27] than in the previous cases, and the picoline bond lengths are indicative of their dative character: d(Mo−N2) = 2.147(5) Å, d(Mo−N3) = 2.131(5) Å.

Angular Distortions: A Walsh Diagram Perspective. Each of the structures characterized above manifests a

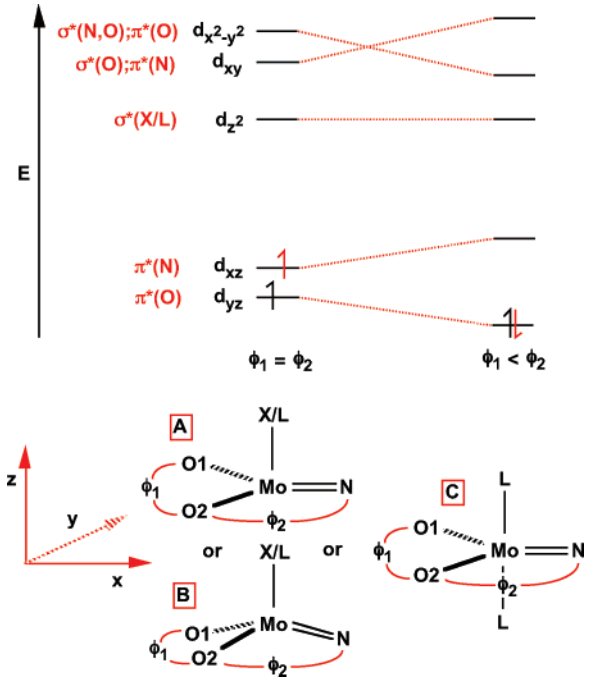

Figure 6. Walsh diagram rationalizing distortions of $(silox)_2ClMo{=}N^tBu$ (**4**-^{t}Bu, **B**, X = Cl, d^1), $[(silox)_2Mo{=}N^tBu]_2Hg$ ((**5**-^{t}Bu)$_2$Hg, **A**, X = Hg, effectively d^1), $(silox)_2(Me_3P)Mo{=}N^tBu$ (**6**-^{t}Bu, **B**, X = PMe_3, d^2), and $(silox)_2(4\text{-pic})_2Mo{=}N^tBu$ (**7**-4-pic, **C**, L = 4-pic, d^2).

relatively "closed" O1−Mo−O2 angle (<120°) with respect to more "open" N═Mo−O1 and N═Mo−O2 angles (>120°), which is opposite of that observed for $(silox)_2W{=}N^tBu$,[19] whose wider O−W−O angle was rationalized on the basis of steric features within the pseudotrigonal plane. The difference is the presence of a fourth, or fourth and fifth in the case of **7**-4-pic, ligand, which changes the electronic structure of the complex in a simple, yet profound way. Taking the additional ligand(s) as binding along *z*, its presence raises the level of d_{z^2}, such that it is no longer the HOMO as it is in $(silox)_2W{=}N^tBu$.

Figure 6 illustrates a Walsh diagram that rationalizes the structural observations. The placement of d_{z2} is somewhat arbitrary but well above the lower two orbitals in contrast to a 3-coordinate manifold. In the pseudotrigonal situation (ϕ_1(O1−Mo−O2) = ϕ_2(N═Mo−O1 and N═Mo−O2), d_{yz} is the lowest orbital in the ligand field, and it is the π^* component of the O(pπ) → Mo(dπ) interaction. Since the N(pπ) → Mo(dπ) interaction is greater than that of the oxygens, its π^* component is the next orbital, d_{xz}, which also carries a small amount of oxygen π^* character. A closing of ϕ_1 with respect to ϕ_2 ($\phi_1 < \phi_2$) attenuates the π^* character of d_{yz} at the expense of the π^* character of d_{xz}, as the oxygens move further away from the *yz*-plane and closer to the *xz*-plane. This is effectively the same scenario whether the system is pseudotrigonal (**A** or **C**) or distorting toward pseudotetrahedral (**B**, pseudo-C_{3v}), although the energy gaps become less pronounced in the latter. There is a subtle, net stabilization for d^1 and d^3 configurations and for d^2 if spin-pairing is achieved. Note that this is consistent with the unusual orientation of the PMe_3 ligand in $(silox)_2(Me_3P)Mo{=}N^tBu$ (**6**-^{t}Bu, **B**), which maximizes π-backbonding via d_{yz}.

Scheme 3

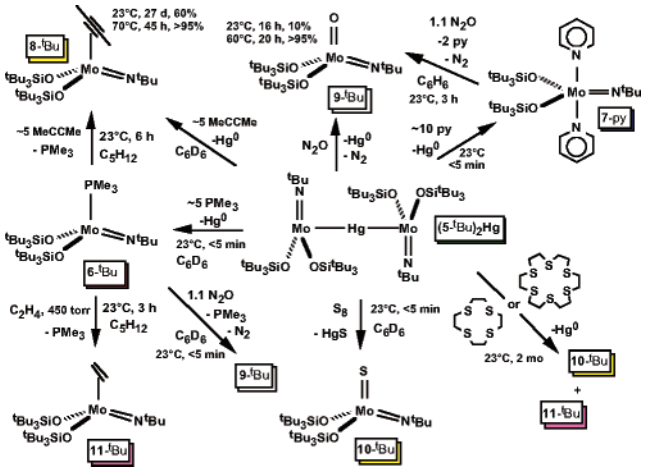

Table 4. Estimated Pseudo-First-Order Rate Constants for Nucleophilic Cleavage of $[(silox)_2Mo{=}N^tBu]_2Hg$ ((**5**-^{t}Bu)$_2$Hg)

nucleophile	*T* (°C)	~$t_{1/2}$ (s)	*k* (s^{-1})
PMe_3	25	45	$1.5(6) \times 10^{-2}$
pyridine	25	45	$1.5(6) \times 10^{-2}$
N_2O	25	4.0×10^5	$1.7(2) \times 10^{-6}$
	60	9.0×10^3	$7.7(1) \times 10^{-5}$
2−butyne	25	1.7×10^6	$4.1(2) \times 10^{-7}$

As ϕ_1 approaches 90°, the σ^* character of d_{xy} will increase, while the corresponding σ^* character of $d_{x^2-y^2}$ decreases. Figure 6 shows these orbitals crossing in energy, but the effect may not be as pronounced.

Reactivity of $[(silox)_2Mo{=}N^tBu]_2Hg$ ((5-^{t}Bu)$_2$Hg). Thermolysis of $[(silox)_2Mo{=}N^tBu]_2Hg$ ((**5**-^{t}Bu)$_2$Hg) in C_6D_6 revealed a surprising stability. Virtually no degradation was noted after 14 d at 60 °C, and at 100 °C, full degradation was only observed after 22 d! When monitored at 140 °C, a degradation rate of roughly $1.09(6) \times 10^{-4}$ s^{-1} was obtained, which corresponds to a $\Delta G^{\ddagger}_{deg}$ = 31.9(1) kcal/mol. This nature of the degradation proved elusive, as ensuing studies showed.

Despite its robust nature, ((**5**-^{t}Bu)$_2$Hg was found to be susceptible to scission by a number of reagents, as Scheme 3 illustrates, and a crude correlation with substrate nucleophilicity was noted when rough half-lives for Mo−Hg bond breaking were tabulated (Table 4). In an excess (10 equiv) of pyridine in C_6D_6, (**5**-^{t}Bu)$_2$Hg was essentially consumed in <5 min to produce $(silox)_2py_2Mo{=}N^tBu$ (**7**-^{t}Bu, 93%) and Hg°, yet when the steric bulk about the nitrogen was increased through the use of 2,6-lutidine,[29] no reaction was observed. The exposure of (**5**-^{t}Bu)$_2$Hg to ~5 equiv of PMe_3 in C_6D_6 afforded $(silox)_2(Me_3P)Mo{=}N^tBu$ (**6**-^{t}Bu) and Hg° within minutes, and the same reactivity was observed for PMe_2Ph and $PMePh_2$, although the products, presumably also phosphine adducts, were not assayed. When 2-butyne (4.8 equiv) was utilized as a substrate, (**5**-^{t}Bu)$_2$Hg showed 59% conversion to the mono-2-butyne adduct after 27 d at 25 °C in C_6D_6, and thermolysis at 70 °C for 45 h completed the

(29) Lutidene should be sterically capable of trapping the 3-coordinate complex. See: Covert, K. J.; Neithamer, D. R.; Zonnevylle, M. C.; LaPointe, R. E.; Schaller, C. P.; Wolczanski, P. T. *Inorg. Chem.* **1991**, *30*, 2494−2508.

conversion to (silox)$_2$(MeCCMe)Mo=N^{t}Bu (**8**-^{t}Bu) with concomitant Hg°.

Nitrous oxide was explored as a possible oxidative cleavage agent, but only 10% formation of (silox)$_2$(O)Mo=N^{t}Bu (**9**-^{t}Bu) was noted after 16 h at 25 °C, despite a significant thermodynamic driving force.[30,31] Thermolysis at 60 °C revealed 87% conversion after 7 h, and in 20 h, all of the (**5**-^{t}Bu)$_2$Hg was replaced with **9**-^{t}Bu and Hg°. In view of this result with a small substrate, it was not surprising that the larger Ph_3PO failed to effect OAT at 25° for 2 weeks.[9,31]

Several attempts were made to remove Hg° from of [(silox)$_2$Mo=N^{t}Bu]$_2$Hg ((**5**-^{t}Bu)$_2$Hg), leaving putative (silox)$_2$-Mo=N^{t}Bu (**5**-^{t}Bu) as the desired product. Exposure of ((**5**-^{t}Bu)$_2$Hg to S_8 (1/8−1 equiv) in C_6D_6 at 25 °C generated 2 equiv of (silox)$_2$(S)Mo=N^{t}Bu (**10**-^{t}Bu) and a black precipitate presumed to be mercuric sulfide (Scheme 3). The use of thiacrown molecules, 1,4,7,10-tetrathiacyclododecane or 1,4,7,10,13,16-hexathiacyclooctadecane, did not generate ionic products when placed in the presence of ((**5**-^{t}Bu)$_2$Hg in C_6D_6 over the course of 5 days. After 2 months, ^{1}H NMR spectroscopy revealed a 1:1 mixture of **10**-^{t}Bu and (silox)$_2$-(C_2H_4)Mo=N^{t}Bu (**11**-^{t}Bu), along with a dark material assumed to be Hg°.

Reactivity of (silox)$_2$(py)$_2$Mo=N^{t}Bu (7-py) and (silox)$_2$-(Me$_3$P)Mo=N^{t}Bu (6-^{t}Bu). In view of the reactivity above, more convenient synthetic routes were sought for some of the derivatives of (silox)$_2$Mo=N^{t}Bu (**5**-^{t}Bu), which itself eluded isolation. Treatment of (silox)$_2$(py)$_2$Mo=N^{t}Bu (**7**-py) or (silox)$_2$ (Me$_3$P)Mo=N^{t}Bu (**6**-^{t}Bu) to a slight excess of N_2O (1.2 equiv) in pentane resulted in effervescence (N_2 loss) and formation of (silox)$_2$(O)Mo=N^{t}Bu (**9**-^{t}Bu) as an off-white solid in ∼80% yield (Scheme 3). When (silox)$_2$-(Me$_3$P)Mo=N^{t}Bu (**6**-^{t}Bu) was exposed to 450 Torr ethylene in hydrocarbon solvent, a color change from maroon to dark pink was noted, and upon crystallization from pentane, dark pink crystals of (silox)$_2$(C_2H_4)Mo=N^{t}Bu (**11**-^{t}Bu) formed in ∼70% yield. Its ^{1}H NMR spectrum indicated two resonances for the bound ethylene ligand (δ 1.83, 2H, δ 2.79, 2H, Table 1), and a single ethylene resonance at δ 52.06 in the ^{13}C{^{1}H} NMR spectrum. Variable-temperature ^{1}H NMR spectroscopy (−50 to 90 °C) revealed a coalescence of the two CH signals at 78 °C, which afforded a rotation barrier of $\Delta G^{\ddagger}_{rot}$ = 15.2(5) kcal mol^{-1}, similar to that of (silox)$_2$W=N^{t}Bu(C_2H_4) ($\Delta G^{\ddagger}_{rot}$ = 15.3 kcal mol^{-1}). (silox)$_2$Mo=N^{t}Bu-(C_2Me_2) (**8**-^{t}Bu) was similarly isolated as a yellow solid in ∼65% yield via the addition of 5 equiv of 2-butyne to a pentane solution of **6**-^{t}Bu. Equivalent Me groups on the 2-butyne (Table 1) in the ^{1}H and ^{13}C{^{1}H} NMR spectra implied a structure where the CC alignment was perpendicular to the imido, akin to **11**-^{t}Bu. This structure is expected for both, since interaction with the filled d_{yz} (Figure 6) orbital constitutes the π-backbonding for ethylene and 2-butyne. Although d_{xz} is empty, the ^{13}C alkyne shift of 179.15 is more consistent with the 2-butyne acting as a simple 2-electron donor, instead of effectively competing with the imide as a π-donor.[32]

Attempts to Prepare (silox)$_2$Mo=N^{t}Bu (5-^{t}Bu) via Atom Abstraction. The failure to prepare (silox)$_2$Mo=N^{t}Bu (**5**-^{t}Bu) by reduction or via the controlled degradation of [(silox)$_2$Mo=N^{t}Bu]$_2$Hg ((**5**-^{t}Bu)$_2$Hg) prompted efforts at generating the 3-coordinate species via atom abstraction. (silox)$_3$Ta was employed to abstract oxygen from (silox)$_2$-(O)Mo=N^{t}Bu (**9**-^{t}Bu) at 23−75 °C, but only cyclometalation to (silox)$_2$HTa(κ-O,C−OSi^{t}BuCMe$_2$CH$_2$)[9] was observed. Next, attempts to abstract Cl from (silox)$_2$ClMo=N^{t}Bu (**4**-^{t}Bu) were tried using (silox)$_3$Ta[33] (25−80 °C) and {(TMS)$_2$N}$_3$Ti[34] (23 °C), but cyclometalation was again seen in the former, and no reaction occurred in the latter case. While it could be argued that the steric demands of these reagents obviated any atom-transfer path, the reduction of (silox)$_3$TaCl$_2$ to (silox)$_3$Ta is believed to occur via disproportionation of (silox)$_3$TaCl,[35] and this process occurs readily at 23 °C. Finally, (silox)$_3$Ta was successfully converted to (silox)$_3$Ta(η^2-N,C-py)[29] in the presence of 1/2 equiv of (silox)$_2$(py)$_2$Mo=N^{t}Bu (**7**-py), but the molybdenum products could not be identified. No ^{1}H NMR spectral shifts could be assigned to **5**-^{t}Bu or plausible degradation products; while **5**-^{t}Bu may be paramagnetic, this should not have prevented its observation, as other paramagnetic molecules in related silox systems have been plainly observable. Frustrated by these efforts to obtain **5**-^{t}Bu or evidence of its existence, calculations were initiated and the curious stability of (**5**-^{t}Bu)$_2$Hg was investigated.

Computational Studies. 1. (HO)$_2$Mo=NH. Since (silox)$_2$Mo=N^{t}Bu (**5**-^{t}Bu) could not be detected, it was computationally modeled as (HO)$_2$Mo=NH (**5′**) using density functional methods, and the d-orbital splitting diagram including orbital energies is depicted in Figure 7. A slightly closed O−Mo−O angle of 117° is predicted from a B3PW91/CEP-31G(d) geometry optimization for planar (triplet) **5′**, with accompanying 120° and 123° O−Mo=N angles. If **5′** is considered to be pseudo-C_{2v}, its ground state is $^3A_2$ (this results from formally aligning the *z*-axis with the Mo=N vector; in Figure 7, the axes were chosen to be comparable to Figure 6, and for visualizing the fragment in a trigonal context) by virtue of its $(d_{z^2})^1(d_{yz})^1$ configuration. The singlet−triplet free energy gaps ($\Delta G_{ST} = \Delta G_T - \Delta G_S$) were determined at various levels of theory and ranged from +0.4 (BLYP/CEP-31G(d)) to −8.2 (BHandHLYP/CEP-31G(d)) kcal/mol, with an average for six functionals at −4(3) kcal/mol. A CCSD(T) single-point energy investigation using the optimized geometry revealed ΔG_{ST} to be −0.7 kcal/mol.[19] The similar energies of the triplet GS and singlet first excited state (ES) are reminiscent of (silox)$_3$Nb, whose model

(30) Cherry, J. P. F.; Johnson, A. R.; Baraldo, L. M.; Tsai, Y. C.; Cummins, C. C.; Kryatov, S. V.; Rybak-Akimova, E. V.; Capps, K. B.; Hoff, C. D.; Haar, C. M.; Nolan, S. P. *J. Am. Chem. Soc.* **2001**, *123*, 7271−7286.
(31) Holm, R. H.; Donahue, J. P. *Polyhedron* **1993**, *12*, 571−593.
(32) Templeton, J. L. *Adv. Organomet. Chem.* **1989**, *29*, 1−100.
(33) Halide abstraction from RX by (silox)$_3$Ta has been studied. Chambers, M.; Chadeayne, A. R.; Wolczanski, P. T. Unpublished results.
(34) Alyea, E. C.; Bradley, D. C.; Copperthwaite, R. G. *J. Chem. Soc., Dalton Trans.* **1972**, 1580−1584.
(35) Chadeayne, A. R.; Wolczanski, P. T.; Lobkovsky, E. B. *Inorg. Chem.* **2004**, *43*, 3421−3432.

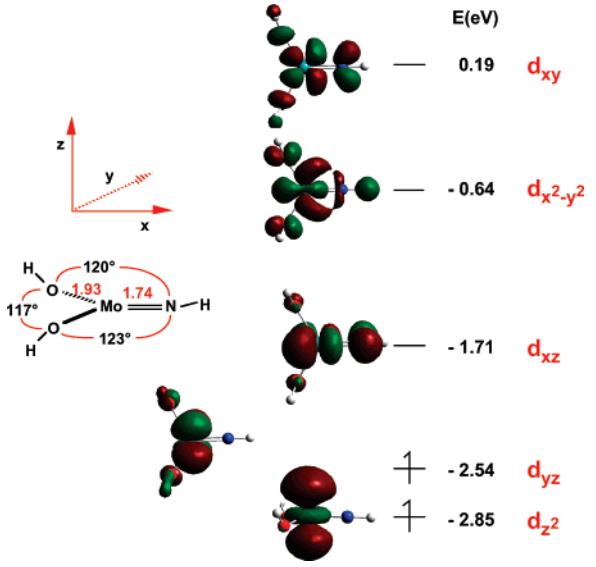

Figure 7. Calculated (B3PW91/CEP-31G(d) functional) d-orbital splitting diagram for $(HO)_2Mo{=}NH$ (**5′**), a model for $(silox)_2Mo{=}NR$ (R = ^{t}Bu, **5**-^{t}Bu; ^{t}Amyl, **5**-^{t}Amyl), at the optimized geometry shown (bond lengths given in red are in Å). The axes have been chosen in the context of trigonal systems; in C_{2v}, the Mo=N vector would be aligned with *z*, and the O_2MoN plane would be *xz*.

$(HO)_3Nb$ was calculated to possess triplet (GS) and singlet states ~2 kcal/mol apart.[9]

The lowest orbital in Figure 7 is d_{z^2}, which is essentially nonbonding, in part because of 5s/4d mixing,[36,37] while the d_{yz} orbital is the next lowest of the d-block, and it is π^* with respect to the oxygens as discussed in regard to Figure 6. It is only 0.31 eV above d_{z^2}, yet d_{xz} is 1.14 eV above d_{z^2} because of its greater π^* character resulting from the N-component from the imido ligand. The σ-antibonding orbitals complete the ligand field, with $d_{x^2-y^2}$, mostly Nσ^*, only 1.07 eV above d_{xz}, while d_{xy} is another 0.83 eV higher because of its Nπ^* character in addition to being O σ^*. The calculations certainly show that π-bonding with the imido group is substantially greater than that with the hydroxide (siloxide) oxygens because of the shorter *d*(MoN), and the better energy match of the nitrogen orbitals with the Mo d-block.

2. $[(HO)_2Mo{=}NH]_2Hg$. An optimized C_{2h} geometry was uncovered for $[(HO)_2Mo{=}NH]_2Hg$ (**5′**$_2$-Hg) via calculations employing the B3PW91/CEP-31G(d) level of theory,[19] and the metric parameters were close to that of $[(silox)_2Mo{=}N^tBu]_2Hg$ ((**5**-^{t}Bu)$_2$Hg). Molybdenum−oxygen bond distances of 1.93 and 1.92 Å, a slightly long *d*(MoHg) of 2.75 Å, and a *d*(Mo=N) of 1.74 Å were obtained. Core N−Mo−O angles of 121 and 118° accompanied a smaller O−Mo−O angle of 115°, verifying the likelihood that the origin of this minor distortion is electronic.

A truncated molecular orbital diagram that focuses on the orbitals involved in Mo_2Hg bonding is illustrated in Figure 8. The $1a_g$ and $2a_g$ orbitals feature the symmetric combination

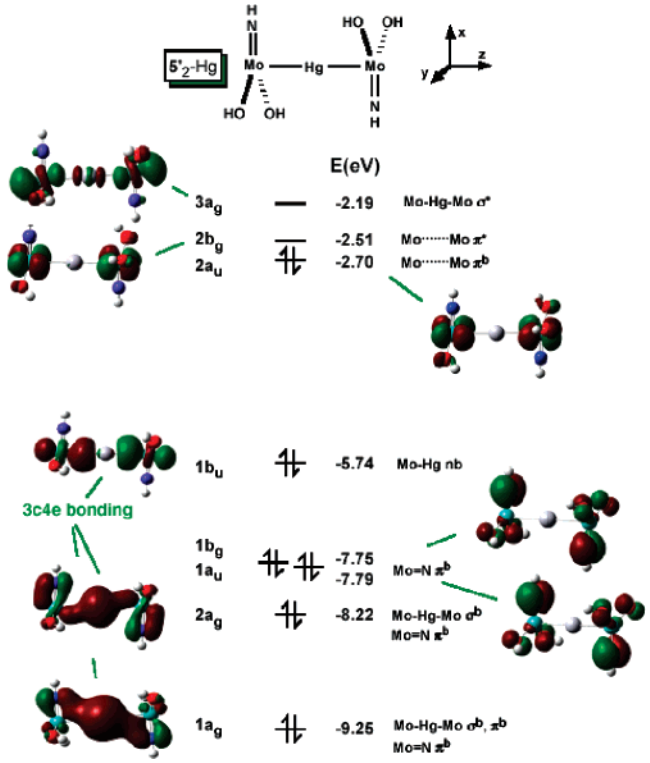

Figure 8. Truncated molecular orbital diagram (B3PW91/CEP-31G(d) functional) for $[(HO)_2Mo{=}NH]_2Hg$ (**5′**), a model for $[(silox)_2Mo{=}NR]_2Hg$ (R = ^{t}Bu, (**5**-^{t}Bu)$_2$Hg; ^{t}Amyl, (**5**-^{t}Amyl)$_2$Hg)), at the optimized geometry shown. The axes have been chosen in the context of trigonal systems; in C_{2h}, the principal axis (*z*) would be normal to the page.

of d_{z^2} orbitals from both $(HO)_2Mo{=}NH$ (**5′**) fragments and the 6s orbital of mercury. The stabilization of $2e^-$ in the σ-framework is spread over these two orbitals because both also manifest Mo=N π^b-character; the lower orbital has the symmetric combination of *xz*-plane Mo=N π- and Mo_2Hg σ-bonding, while the upper orbital has the antisymmetric component. The antisymmetric combination of d_{z^2} orbitals attributed to $(HO)_2Mo{=}NH$ (**5′**) is present as $1b_u$, a nonbonding molecular orbital with essentially no Hg $6p_z$ component. Noting that the $2e^-$ in the Mo_2Hg (d_{z^2} + 6s + d_{z^2}) σ-bonding is spread over two orbitals, the ($1a_g$ + $2a_g$) and $1b_u$ orbitals constitute a 3c4e bonding arrangement that may aid in understanding the reactivity of $[(silox)_2Mo{=}NR]_2Hg$ (R = ^{t}Bu, (**5**-^{t}Bu)$_2$Hg; ^{t}Amyl, (**5**-^{t}Amyl)$_2$Hg).

In between the $2a_g$ and $1b_u$ orbitals are two Mo=N π^b-orbitals, symmetric and antisymmetric, in the *xy*-planes of each pseudotrigonal $(HO)_2Mo{=}NH$ (**5′**) fragment. Separated by the Hg atom, these π^b-orbitals reside at essentially the same energy, ~ −7.8 eV. The frontier orbitals **5′**$_2$-Hg are the Mo···Mo π^b (d_{yz} − d_{yz}) and π^* (d_{yz} + d_{yz}) orbitals ($2a_u$ and $2b_g$) whose components are held distant by the Hg atom, whose $6p_y$ orbital is too high in energy to partake in the bonding of $2a_u$. The 0.19 eV gap between these orbitals at −2.70 and −2.51 eV permits population of each by 1e at room temperature. The ^3B_u excited state is close enough (~550 cm^1) to the ^1A_g ground state to provide the mixing that is manifested in the aforementioned TIP. The four states derived from these proximate orbitals ($(1a_u)^2 \rightarrow {}^1A_g$; $(1a_u)^1$-$(1b_g)^1 \rightarrow {}^3B_u$, ^1B_u; $(1b_g)^2 \rightarrow {}^1A_g$) provide the key estimate of

(36) Soo, H. S.; Figueroa, J. S.; Cummins, C. C. *J. Am. Chem. Soc.* **2004**, *126*, 11370−11376.
(37) Oxtoby, D. W.; Gillis, H. P.; Nachtrieb, N. H., *Principles of Modern Chemistry*, 5th Ed.; Thomson Brooks/Cole: United States, 2002. For a plot of orbital energies vs *Z*, see Figure 15.39 in this ref.

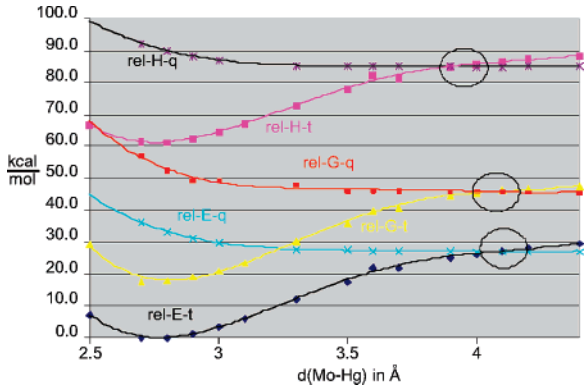

Figure 9. Relative *E* (energy), *G* (free energy), and *H* (enthalpy) triplet and quintet surfaces (B3PW91/CEP-31G(d) functional, kcal/mol) of [(HO)$_2$Mo═NH]$_2$Hg (**5′**), a model for [(silox)$_2$Mo═NR]$_2$Hg (R = ^{t}Bu, (**5**-^{t}Bu)$_2$Hg; ^{t}Amyl, (**5**-^{t}Amyl)$_2$Hg)), as a function of *d*(Mo−Hg) from 2.5 to 4.5 Å. The triplet−quintet crossing points are circled.

the exchange energy necessary to assess the MoMo π-bond energy, as previously described.[19]

To provide insight into the reactivity of [(silox)$_2$Mo═NR]$_2$Hg (R = ^{t}Bu, (**5**-^{t}Bu)$_2$Hg; ^{t}Amyl, (**5**-^{t}Amyl)$_2$Hg), the Mo−Hg bond dissociation energies of [(HO)$_2$Mo═NH]$_2$Hg (**5′**$_2$-Hg) were calculated. It is worth reiterating that the Stevens effective core potentials are derived from relativistic wave functions and thus incorporate scalar relativistic effects and (in an average way) spin−orbit coupling. To keep the calculations from being unwieldy and noting that the single and triplet states of **5′**$_2$-Hg were at essentially the same energy, the triplet state was chosen as the reference, and the calculations were conducted using B3PW91/CEP-31G(d). Equations 1−3 provide the pertinent enthalpic data and reveal that the first *D*(MoHg) is only 22.4 kcal/mol. The *D*(MoHg) of the product mercury adduct, [(HO)$_2$Mo═NH]Hg (**5′**-Hg), is a mere 3.1 kcal/mol, and the total dissociation enthalpy for Hg loss is 25.5 kcal/mol. The calculated low Mo−Hg

$$^3[(HO)_2Mo{=}NH]_2Hg \rightarrow {}^3(HO)_2Mo{=}NH + {}^3[(HO)_2Mo{=}NH]Hg \quad \Delta H = 22.4 \text{ kcal/mol} \quad (1)$$
(**5′**$_2$−Hg → **5′** + **5′**−Hg)

$$^3[(HO)_2Mo{=}NH]Hg \rightarrow {}^3(HO)_2Mo{=}NH + {}^1Hg \quad \Delta H = 3.1 \text{ kcal/mol} \quad (2)$$
(**5′**−Hg → **5′** + ^{1}Hg)

$$^3[(HO)_2Mo{=}NH]_2Hg \rightarrow 2\,{}^3(HO)_2Mo{=}NH\ (\mathbf{5'}) + {}^1Hg \quad \Delta H = 25.5 \text{ kcal/mol} \quad (3)$$
(**5′**$_2$−Hg → 2**5′** + ^{1}Hg)

bond strengths help enthalpically rationalize the generation of the trinuclear derivatives, [(silox)$_2$Mo═NR]$_2$Hg (R = ^{t}Bu, (**5**-^{t}Bu)$_2$Hg; ^{t}Amyl, (**5**-^{t}Amyl)$_2$Hg) from (silox)$_2$Mo═NR (R = ^{t}Bu, **5**-^{t}Bu; ^{t}Amyl, **5**-^{t}Amyl) in the presence of atomic mercury.

3. Reaction Coordinate for Dissociation of [(HO)$_2$Mo═NH]$_2$Hg (5′$_2$-Hg). The reaction coordinate for dissociation of [(HO)$_2$Mo═NH]$_2$Hg (**5′**$_2$-Hg) along the Mo−Hg vector was explored as shown in Figure 9. Triplet and quintet relative energy (*E*), free energy (*G*), and enthalpy (*H*) surfaces are plotted for **5′**$_2$-Hg as a function of *d*(Mo−Hg) from 2.5 to 4.5 Å. The quintet surfaces are "unbound" at the calculated ground-state *d*(Mo−Hg) of 2.75 Å but constitute the ground-state surface of the initial products, (HO)$_2$Mo═NH (**5′**) and [(HO)$_2$Mo═NH]Hg (**5′**-Hg), which are both triplets. The minimum activation *E*, *G*, and *H* can be estimated by assuming an adiabatic transfer from the GS triplet to the quintet surfaces at their respective crossing points. From the graph, the $\Delta E^{\ddagger}$ is ∼27 kcal/mol, and as expected, it is roughly the same as the $\Delta G^{\ddagger}$ of ∼28 kcal/mol. What is surprising for an essentially *dissociative event* is that the $\Delta H^{\ddagger}$ is substantially less than that of the free energy of activation at ∼24 kcal/mol. The latter is in line with the calculated BDE of 22.4 kcal/mol (eq 1) and suggests a modest amount of reorganization from the crossing point to the products. The higher $\Delta E^{\ddagger}$ and $\Delta G^{\ddagger}$ values suggest that the electronic reorganization of **5′**$_2$-Hg, that is, the electronic correlation of **5′**$_2$-Hg to the triplet products **5′** and **5′**-Hg, is a significant contributor. While one might consider this as a consequence of spin state, it is highly unlikely, especially with Hg present, that a change in spin represents a serious energy consideration. However, the orbital symmetry of the Mo(IV) products is each $\pi^1\pi^1$ (i.e., $(d_{xz})^1(d_{yz})^1$), and this contrasts greatly with the $\sigma^2\pi^1\pi^1$ orbital symmetry of **5′**$_2$-Hg. Given our earlier experimental/theoretical analysis of NO scission by related group 5 species, the difficulty in mixing σ- and π-type orbitals is likely to present a serious electronic reorganization barrier in the decomposition of (**5**-R)$_2$Hg.[9]

Thermal Degradation of [(silox)$_2$Mo═NR]$_2$Hg (R = ^{t}Bu, (5-^{t}Bu)$_2$Hg; ^{t}Amyl, (5-^{t}Amyl)$_2$Hg). 1. Initial Observations. The above calculations suggested that the stability accorded [(silox)$_2$Mo═N^{t}Bu]$_2$Hg ((**5**-^{t}Bu)$_2$Hg) was in mild disagreement with the low BDE of the first molybdenum−mercury bond and that electronic factors, perhaps assessable via measurement of a large negative entropy of activation, might play a critical role. Thermolysis of [(silox)$_2$Mo═N^{t}Bu]$_2$Hg ((**5**-^{t}Bu)$_2$Hg) at 60 °C in C_6D_6 for 14 h afforded no noticeable degradation, but after 22 d at 100 °C, its destruction was accompanied by a plethora of products. If the calculated bond enthalpy for dissociation or Mo−Hg bond cleavage in (**5**-^{t}Bu)$_2$Hg is taken as an estimate of $\Delta G^{\ddagger}$ as 22.4 kcal/mol (eq 1), the rate constant for dissociation at 25 °C would be 2.4×10^{-4} s^{-1} and $t_{1/2} \approx 50$ min; at 60 °C, $k_{60} \approx 1.4 \times 10^{-2}$ s^{-1} and $t_{1/2} \approx 50$ s, and at 100 °C, $k_{100} \approx 0.6$ s^{-1} and $t_{1/2} \approx 1$ s. Clearly the actual degradation behavior is well outside these parameters.

To undertake a more careful study on a convenient time scale, [(silox)$_2$Mo═N^{t}Bu]$_2$Hg ((**5**-^{t}Bu)$_2$Hg) was heated at 140 °C to yield an average degradation rate of $1.09(6) \times 10^{-4}$, with a $\Delta G^{\ddagger}_{140}$ of 31.9(1) kcal/mol that is well above a value predicated on a simple dissociation. If the system behaved as expected, that is, with $\Delta S^{\ddagger} > 0$, then the enthalpy of activation would be well above 32 kcal/mol, a value significantly larger than that implied by eq 1. Unfortunately, the decay of (**5**-^{t}Bu)$_2$Hg as displayed by a ln[(**5**-^{t}Bu)$_2$Hg] versus time plot was somewhat irregular but only credibly fit by a first-order process.

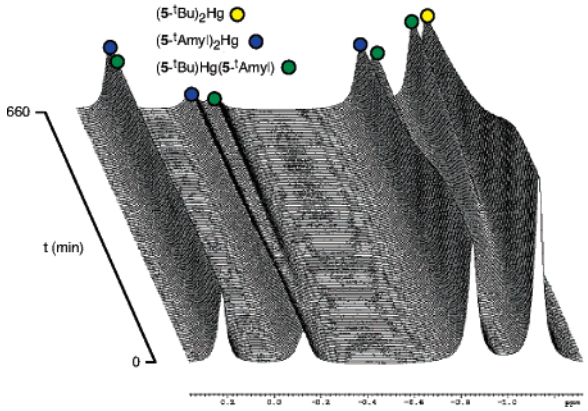

Figure 10. Stacked plot of ^{1}H NMR spectra for the crossover of [(silox)$_2$Mo=N^{t}Bu]$_2$Hg ((**5**-^{t}Bu)$_2$Hg, yellow) and [(silox)$_2$Mo=NC(Me)$_2$Et]$_2$Hg ((**5**-^{t}Amyl)$_2$Hg, blue) showing the growth of [(silox)$_2$Mo=N^{t}Bu]Hg-[(silox)$_2$MoN^{t}Amyl] ((**5**-^{t}Bu)Hg(**5**-^{t}Amyl), green) in the region from 0.3 to −1.3 ppm.

2. Crossover of [(silox)$_2$Mo=N^{t}Bu]$_2$Hg ((5-^{t}Bu)$_2$Hg) and [(silox)$_2$Mo=N^{t}Amyl]$_2$Hg ((5-^{t}Amyl)$_2$Hg). In view of the unexpected stability and erratic "first-order" degradation of [(silox)$_2$Mo=N^{t}Bu]$_2$Hg ((**5**-^{t}Bu)$_2$Hg), the possibility of a reversible cleavage as shown in eqs 4 and 5 was considered. While it seemed unlikely that a ternary system of two

$$\underset{(\mathbf{5}-{}^t\mathrm{Bu})_2\mathrm{Hg}}{[(\mathrm{silox})_2\mathrm{Mo}{=}\mathrm{N}^t\mathrm{Bu}]_2\mathrm{Hg}} \rightleftarrows \underset{\mathbf{5}-{}^t\mathrm{Bu}}{(\mathrm{silox})_2\mathrm{Mo}{=}\mathrm{N}^t\mathrm{Bu}} + \underset{(\mathbf{5}-{}^t\mathrm{Bu})\mathrm{Hg}}{[(\mathrm{silox})_2\mathrm{Mo}{=}\mathrm{N}^t\mathrm{Bu}]\mathrm{Hg}} \quad (4)$$

$$\underset{(\mathbf{5}-{}^t\mathrm{Bu})_2\mathrm{Hg}}{[(\mathrm{silox})_2\mathrm{Mo}{=}\mathrm{N}^t\mathrm{Bu}]\mathrm{Hg}} \rightleftarrows \underset{\mathbf{5}-{}^t\mathrm{Bu}}{(\mathrm{silox})_2\mathrm{Mo}{=}\mathrm{N}^t\mathrm{Bu}} + \mathrm{Hg} \quad (5)$$

(silox)$_2$Mo=N^{t}Bu (**5**-^{t}Bu) and Hg would reform at 140 °C, it would at least explain the apparent robust nature of (**5**-^{t}Bu)$_2$Hg. Such an occurrence was probed via a crossover study involving (**5**-^{t}Bu)$_2$Hg and [(silox)$_2$Mo=NC(Me)$_2$Et]$_2$Hg ((**5**-^{t}Amyl)$_2$Hg, eq 6).

$$\underset{(\mathbf{5}-{}^t\mathrm{Bu})_2\mathrm{Hg}}{[(\mathrm{silox})_2\mathrm{Mo}{=}\mathrm{N}^t\mathrm{Bu}]_2\mathrm{Hg}} + \underset{(\mathbf{5}-{}^t\mathrm{Amyl})_2\mathrm{Hg}}{[(\mathrm{silox})_2\mathrm{Mo}{=}\mathrm{N}^t\mathrm{Amyl}]_2\mathrm{Hg}} \rightleftarrows \underset{(\mathbf{5}-{}^t\mathrm{Bu})\mathrm{Hg}(\mathbf{5}-{}^t\mathrm{Amyl})}{2[(\mathrm{silox})_2\mathrm{Mo}{=}\mathrm{N}^t\mathrm{Bu}]\mathrm{Hg}[(\mathrm{silox})_2\mathrm{Mo}{=}\mathrm{N}^t\mathrm{Amyl}]} \quad (6)$$

An equimolar mixture (~0.00140 M each) of (**5**-^{t}Bu)$_2$Hg and (**5**-^{t}Amyl)$_2$Hg dissolved in benzene-d_6 afforded a statistical mixture containing the crossover product [(silox)$_2$Mo=N^{t}Bu]Hg[(silox)$_2$Mo=N^{t}Amyl] ((**5**-^{t}Bu)Hg(**5**-^{t}Amyl)) after 11 h, as Figure 10 clearly shows. Fortunately, the CH$_2$ and Me groups on (**5**-^{t}Amyl)$_2$Hg and (**5**-^{t}Bu)Hg(**5**-^{t}Amyl)) were distinct, as were the imide ^{t}Bu groups of (**5**-^{t}Bu)$_2$Hg and the crossover product. Line-fitting experiments had to be performed to obtain concentrations because the overlap between the ^{1}H NMR resonances obviated standard integration procedures. With crossover occurring this rapidly at 11 h, a rough half-life of 5 h would correspond to a $\Delta G^{\ddagger}$ for dissociation of ~23 kcal/mol, which was essentially the expected value based on the calculated Mo−Hg BDE.

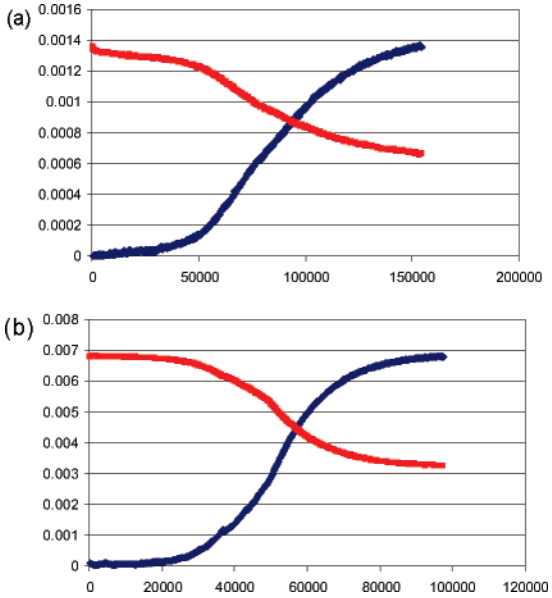

Figure 11. Two concentration vs time profiles of [(silox)$_2$Mo=N^{t}Bu]$_2$Hg ((**5**-^{t}Bu)$_2$Hg) and [(silox)$_2$Mo=N^{t}Amyl]$_2$Hg ((**5**-^{t}Amyl)$_2$Hg crossover to give [(silox)$_2$Mo=N^{t}Bu]Hg-[(silox)$_2$MoN^{t}Amyl] ((**5**-^{t}Bu)Hg(**5**-^{t}Amyl)). The red line corresponds to [(**5**-^{t}Bu)$_2$Hg] = [(**5**-^{t}Amyl)$_2$Hg] and the blue line to [(**5**-^{t}Bu)Hg(**5**-^{t}Amyl)], and the time line is in seconds. In panel a, the t = 0 s concentrations are 0.00136 M; the induction period is ~45 000 s (~12 h), and full crossover is estimated to be at 170 000 s (47 h): run 1 in Table 5. In b, the t = 0 s concentrations of (**5**-^{t}Bu)$_2$Hg) and (**5**-^{t}Amyl)$_2$Hg are 0.00680 M; the induction period is ~23 000 s (7 h), and crossover is achieved ~95 000 s (26 h): run 6 in Table 5.

However, a closer inspection of the stacked plot indicated that the growth of the crossover product and the concomitant decay of (**5**-^{t}Bu)$_2$Hg and (**5**-^{t}Amyl)$_2$Hg were *not* smooth; an induction region was present, prompting a more detailed kinetics investigation of the exchange process.

Figure 11a exhibits a concentration versus time profile of a [(**5**-^{t}Bu)$_2$Hg] = [(**5**-^{t}Amyl)$_2$Hg] = 0.00140 M crossover run in which the induction period was roughly ~12 h and crossover to a statistical distribution was achieved in ~47 h at 25(1) °C. The concentration was increased by a factor of 5 in Figure 11b to 0.00680 M, and the induction period was ~7 h with crossover completed in ~26 h. Attempts to model the degradation via a variety of pathways proved unsatisfactory, so the reaction profile was broken up into two regimes for easier examination. The first was the induction period, which was treated via initial rate estimations as a first-order decay. Table 5 reveals that the [(**5**-^{t}Bu)$_2$Hg] decay is ~10^{-8} to 10^{-9} s^{-1} and is roughly mirrored by the growth of crossover product in that region. The rate constant corresponds to a $\Delta G^{\ddagger}$ of 29 kcal/mol, a value that corresponds reasonably to the original "degradation rate" when factors such as the lower temperature (25 °C) and the negative entropy of activation implicated by the calculations are included.

To simply assess the crossover region following the induction period, half-lives were taken when [(**5**-^{t}Bu)$_2$Hg]$_t$ = [(**5**-^{t}Bu)$_2$Hg]$_0$/2, and the accompanying rate constants were checked for concentration dependencies. Care was taken to choose the onset of the second kinetics regime as consistently as possible from run to run. With the exception of run 6 (Table 5), the data is most consistent with a −d[(**5**-^{t}Bu)$_2$Hg]/

Table 5. Concentration Dependent and Hg° Addition Studies of [(silox)$_2$Mo=N^{t}Bu]$_2$Hg ((**5**-^{t}Bu)$_2$Hg) and [(silox)$_2$Mo=N^{t}Amyl]$_2$Hg ((**5**-^{t}Amyl)$_2$Hg Crossover to give [(silox)$_2$Mo=N^{t}Bu]Hg[(silox)$_2$MoN^{t}Amyl] ((**5**-^{t}Bu)Hg(**5**-^{t}Amyl))[a]

run	[(**5**-^{t}Bu)$_2$Hg] (mM)	induction[b] (s^{-1})	k_{obs}[c] (s^{-1})	crossover[d] $t_{1/2}$ (s)	$k_{obs,1/2\ order}$[e] ($M^{1/2}s^{-1}$)	$k_{obs,first\ order}$[f] (s^{-1})	$k_{obs,3/2\ order}$[g] ($M^{-1/2}s^{-1}$)	$k_{obs,secondorder}$[h] ($M^{-1}s^{-1}$)
1	1.36	45 600	$1.43(5) \times 10^{-9}$	39000	$5.5(4) \times 10^{-7}$	$1.7(1) \times 10^{-5}$	$5.6(4) \times 10^{-4}$	$1.9(1) \times 10^{-2}$
2	1.36	47 400	$1.29(4) \times 10^{-9}$	41500	$5.2(2) \times 10^{-7}$	$1.6(1) \times 10^{-5}$	$4.2(4) \times 10^{-4}$	$1.7(2) \times 10^{-2}$
3	3.51	9000	NA	21400	$1.6(2) \times 10^{-6}$	$3.2(4) \times 10^{-5}$	$6.4(12) \times 10^{-4}$	$1.3(3) \times 10^{-2}$
4	3.51	9600	$7.1(6) \times 10^{-9}$	20500	$1.7(8) \times 10^{-6}$	$3.4(2) \times 10^{-5}$	$6.8(8) \times 10^{-4}$	$1.4(1) \times 10^{-2}$
5	6.80	10 800	$1.1(1) \times 10^{-8}$	13800	$3.5(2) \times 10^{-6}$	$5.0(1) \times 10^{-5}$	$7.2(4) \times 10^{-4}$	$1.0(1) \times 10^{-2}$
6	6.80	22 800	$2.1(1) \times 10^{-9}$	33500	$1.4(1) \times 10^{-6}$	$2.0(2) \times 10^{-5}$	$3.0(3) \times 10^{-4}$	$4.5(2) \times 10^{-3}$

run	[(**5**-^{t}Bu)$_2$Hg] (mM)	solvent	Hg° added	induction period[b] (s)
7	3.90	Hg° sat'd C_6D_6	none	10 600
8	3.90	Hg° sat'd C_6D_6	0.05 mL	9300
9	3.90	C_6D_6	0.05 mL	11 200
10	3.90	C_6D_6	none	8000
11	3.90	C_6D_6	none	6800

[a] All crossover studies performed with $[(\mathbf{5}\text{-}^t\text{Bu})_2\text{Hg}]_0 = [(\mathbf{5}\text{-}^t\text{Amyl})_2\text{Hg}]_0$. [b] From $t = 0$ s, until deviation in curvature was noted. [c] First-order decay was assumed. [d] Time at which $[(\mathbf{5}\text{-}^t\text{Bu})_2\text{Hg}] = [(\mathbf{5}\text{-}^t\text{Amyl})_2\text{Hg}] = [(\mathbf{5}\text{-}^t\text{Bu})_2\text{Hg}]_0/2 = [(\mathbf{5}\text{-}^t\text{Amyl})_2\text{Hg}]_0/2$. [e] From $-d[(\mathbf{5}\text{-}^t\text{Bu})_2\text{Hg}]/dt = k_{obs}[(\mathbf{5}\text{-}^t\text{Bu})_2\text{Hg}]^{1/2}$ and the observation of $t_{1/2} = (2 - 2^{1/2})[(\mathbf{5}\text{-}^t\text{Bu})_2\text{Hg}]_0^{1/2}/k_{obs}$. [f] From $-d[(\mathbf{5}\text{-}^t\text{Bu})_2\text{Hg}]/dt = k_{obs}[(\mathbf{5}\text{-}^t\text{Bu})_2\text{Hg}]$ and the observation of $t_{1/2} = \ln 2/k_{obs}$. [g] From $-d[(\mathbf{5}\text{-}^t\text{Bu})_2\text{Hg}]/dt = k_{obs}[(\mathbf{5}\text{-}^t\text{Bu})_2\text{Hg}]^{3/2}$ and the observation of $t_{1/2} = (2(2)^{1/2} - 2)/[(\mathbf{5}\text{-}^t\text{Bu})_2\text{Hg}]_0^{1/2}k_{obs}$. [h] From $-d[(\mathbf{5}\text{-}^t\text{Bu})_2\text{Hg}]/dt = k_{obs}[(\mathbf{5}\text{-}^t\text{Bu})_2\text{Hg}]^2$ and the observation of $t_{1/2} = 1/[(\mathbf{5}\text{-}^t\text{Bu})_2\text{Hg}]_0k_{obs}$.

$dt = k_{obs}[(\mathbf{5}\text{-}^t\text{Bu})_2\text{Hg}]^{3/2}$ expression, since the 3/2-order rate constants show only a very modest increase of 30% as [(**5**-^{t}Bu)$_2$Hg] is quintupled. As the concentration of (**5**-^{t}Bu)$_2$Hg is increased, the half-order and first-order rate constants clearly increase, and the second-order k_{obs} values decline. However, the portrayal of the "crossover region" as 3/2-order must be taken as tentative given the outlying nature of run 6, which is distinctly numerically different from all other runs but consistent in appearance (Figure 11b.).

Attempts were made to hasten the crossover through the addition of ligands that initiate the degradation of [(silox)$_2$Mo=N^{t}Bu]$_2$Hg ((**5**-^{t}Bu)$_2$Hg) and [(silox)$_2$Mo=NC(Me)$_2$Et]$_2$Hg ((**5**-^{t}Amyl)$_2$Hg). The addition of L = PMe_3 and pyridine, added in 0.1−0.2 equiv, were chosen to cleave the Hg−Mo bond and generate free (silox)$_2$Mo=NR (R = ^{t}Bu, **5**-^{t}Bu; ^{t}Amyl, **5**-^{t}Amyl), which were considered logical candidates as intermediates in the crossover reaction. Unfortunately, both the PMe_3 and py proved to be too effective at scavenging the putative 3-coordinate species, and the crossover reaction was unchanged, save for the formation of (silox)$_2$LMo=NR. A few experiments were conducted with Hg-saturated C_6D_6 as the solvent ([Hg] ≈ 10^{-7} M, estimated from vapor pressure), with and without Hg° present (runs 7−9), and their induction periods proved to be slightly longer than runs without added Hg° that used the same batch of starting material (runs 10 and 11). If the degradation of (**5**-^{t}Bu)$_2$Hg and (**5**-^{t}Amyl)$_2$Hg were reversible, the addition of Hg may help prolong the induction period.

The observation of crossover (eq 6 and Figures 10 and 11) suggests that intact (silox)$_2$Mo=NR (R = ^{t}Bu, **5**-^{t}Bu; ^{t}Amyl, **5**-^{t}Amyl) compounds are exchanging and that the Hg-containing binuclear complexes can reform, *but this need not be the case*. As Figure 12 illustrates, the exchange of imido groups and even silox groups could occur via intact trinuclear compounds or through **5**-R (R = ^{t}Bu, ^{t}Amyl) exchange with a binuclear via bridging imido or bridging siloxide transition states (or intermediates). The synthesis of the bridging imido molybdenum double-bonded dimer

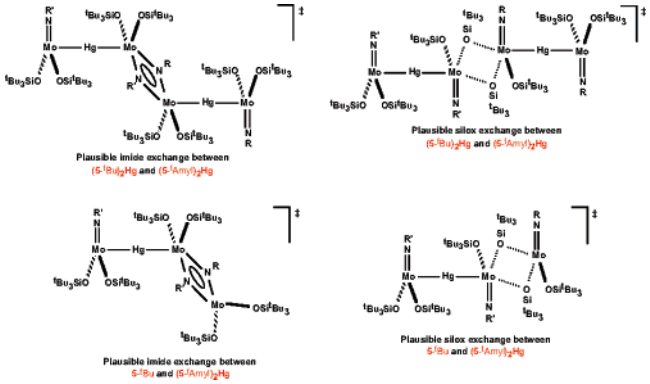

Figure 12. Plausible transition states for imide/imide and silox/silox exchange between trinuclear species and between mononuclear and trinuclear compounds.

$[Mo(=NAr)(O\text{-}t\text{-}Bu)_2]_2$ resulted from the decomposition of $Mo(CH_2CH_2CH_2)(NAr)(O\text{-}t\text{-}Bu)_2$ (Ar = 2,6-*i*-$Pr_2C_6H_3$).[38] Decomposition of W(NAr)(CH-*t*-Bu)(CH_2-*t*-Bu)(OC_6F_5) resulted in the formation of the centrosymmetric heterochiral double-bonded dimer, $[W(=NAr)(CH_2\text{-}t\text{-}Bu)(OC_6F_5)]_2$ (Ar = 2,6-*i*-$Pr_2C_6H_3$).[39,40] Exchange of imido groups between two tetrahedral molybdenum complexes has been observed.[41] Furthermore, the fact that (silox)$_2$W=N^{t}Bu exists only as a monomer[16,17] supports the premise that bridging siloxide or bridging imide complexes are unlikely to be observable.

3. Double-Labeled Crossover of [(silox)$_2$MoN^{t}Bu]$_2$Hg ((5-^{t}Bu)$_2$Hg) and [(silox-*d*$_9$)$_2$MoN^{t}Amyl]$_2$Hg ((5-^{t}Amyl)$_2$Hg-*d*$_{36}$). The crossover results above were unexpected and

(38) Robbins, J.; Bazan, G. C.; Murdzek, J. S.; O'Regen, M. B.; Schrock, R. R. *Organometallics* **1991**, *10*, 2902−2907.
(39) Lopez, L. P. H.; Schrock, R. R. *J. Am. Chem. Soc.* **2004**, *126*, 9526−9527.
(40) (a) Lopez, L. P. H.; Schrock, R. R.; Muller, P. *Organometallics* **2006**, *25*, 1978−1986. (b) Arndt, S.; Schrock, R. R.; Muller, P. *Organometallics* **2007**, *26*, 1279−1290.
(41) (a) Jolly, M.; Mitchell, J. P.; Gibson, V. C. *J. Chem. Soc., Dalton Trans.* **1992**, 1329−1330. (b) Jolly, M.; Mitchell, J. P.; Gibson, V. C. *J. Chem. Soc., Dalton Trans.* **1992**, 1331−1332. (c) Gibson, V. C.; Graham, A. J.; Jolly, M.; Mitchell, J. P. *J. Chem. Soc., Dalton Trans.* **2003**, 4457−4465.

prompted an additional study that used the double-labeled $[(silox\text{-}d_9)_2MoN^tAmyl]_2Hg$ ($(\mathbf{5}\text{-}^tAmyl)_2Hg\text{-}d_{36}$) as a probe. As shown in eq 7, if the crossover of $[(silox)_2Mo{=}N^tBu]_2Hg$ ($(\mathbf{5}\text{-}^tBu)_2Hg$) and $(\mathbf{5}\text{-}^tAmyl)_2Hg\text{-}d_{36}$ afforded only $[(silox)_2Mo{=}N^tBu]Hg[(silox\text{-}d_9)_2MoN^tAmyl]$ ($(\mathbf{5}\text{-}^tBu)Hg(\mathbf{5}\text{-}^tAmyl\text{-}d_{18})$) as the crossover product, then it would be strong evidence that the pseudotrigonal molybdenum fragments were exchanging intact; reversible Mo−Hg−Mo bond formation would be a justifiable conclusion. If, in addition to $(\mathbf{5}\text{-}^tBu)Hg(\mathbf{5}\text{-}^tAmyl\text{-}d_{18})$, exchange products $[(silox)_2Mo{=}N^tBu]Hg[(silox)_2MoN^tAmyl]$ ($(\mathbf{5}\text{-}^tBu)Hg(\mathbf{5}\text{-}^tAmyl)$) and $[(silox\text{-}d_9)_2Mo{=}N^tBu]Hg[(silox\text{-}d_9)_2MoN^tAmyl]$ ($(\mathbf{5}\text{-}^tBu\text{-}d_{18})Hg(\mathbf{5}\text{-}^tAmyl\text{-}d_{18})$) were formed (eq 8), then reversible

$$\underset{(\mathbf{5}-^tBu)_2Hg}{[(silox)_2Mo{=}N^tBu]_2Hg} + \underset{(\mathbf{5}\text{-}^tAmyl)_2Hg\text{-}d_{36}}{[(silox\text{-}d_9)_2MoN^tAmyl]_2Hg} \rightleftarrows 2\,\underset{(\mathbf{5}\text{-}^tBu)Hg(\mathbf{5}\text{-}^tAmyl\text{-}d_{18})}{[(silox)_2Mo{=}N^tBu]Hg[(silox\text{-}d_9)_2MoN^tAmyl]} \quad (7)$$

$$\underset{(\mathbf{5}\text{-}^tBu)_2Hg}{[(silox)_2Mo{=}N^tBu]_2Hg} + \underset{(\mathbf{5}\text{-}^tAmyl)_2Hg\text{-}d_{36}}{[(silox\text{-}d_9)_2MoN^tAmyl]_2Hg} \rightleftarrows \quad (8)$$

$$[(silox)_2Mo{=}N^tBu]Hg[(silox)_2MoN^tAmyl] + (\mathbf{5}\text{-}^tBu)Hg(\mathbf{5}\text{-}^tAmyl) \rightleftarrows [(silox\text{-}d_9)_2Mo{=}N^tBu]Hg[(silox\text{-}d_9)_2MoN^tAmyl] + (\mathbf{5}\text{-}^tBu\text{-}d_{18})Hg(\mathbf{5}\text{-}^tAmyl\text{-}d_{18})$$

generation of the trinuclear complexes would be moot because a simple imido/imido exchange (Figure 12) could account for the products.

While the experiment is in principle a simple one, the analytical methodology is essentially limited to mass spectrometry, where compounds of this ilk are often difficult to assay. The isotopic and ^{t}Bu versus ^{t}Amyl substitutions were chosen for reasonable mass separation. Fortunately, only single Mo centers need to be assessed, because the respective PMe_3 cleavage products of eqs 7 and 8 are distributed

$$(\mathbf{5}\text{-}^tBu)_2Hg + (\mathbf{5}\text{-}^tAmyl)_2Hg\text{-}d_{36} + (\mathbf{5}\text{-}^tBu)Hg(\mathbf{5}\text{-}^tAmyl\text{-}d_{18}) \xrightarrow[-Hg^\circ]{PMe_3}$$

$$\underset{\mathbf{6}\text{-}^tBu}{(silox)_2(Me_3P)Mo{=}N^tBu} + \underset{\mathbf{6}\text{-}^tAmyl\text{-}d_{18}}{(silox\text{-}d_9)_2(Me_3P)Mo{=}N^tAmyl} \quad (9)$$

$$(\mathbf{5}\text{-}^tBu)_2Hg + (\mathbf{5}\text{-}^tAmyl)_2Hg\text{-}d_{36} + (\mathbf{5}\text{-}^tBu)Hg(\mathbf{5}\text{-}^tAmyl) + (\mathbf{5}\text{-}^tBu\text{-}d_{18})Hg(\mathbf{5}\text{-}^tAmyl\text{-}d_{18}) \xrightarrow[-Hg^\circ]{PMe_3}$$

differently. The Mo-containing cleavage products of the equilibria in eq 7 will be a 1:1 mixture of $(silox)_2(Me_3P)Mo{=}N^tBu$ ($\mathbf{6}\text{-}^tBu$) and $(silox\text{-}d_9)_2(Me_3P)Mo{=}N^tAmyl$ ($\mathbf{6}\text{-}^tAmyl\text{-}d_{18}$, eq 9), whereas the products derived from eq 8 would include $\mathbf{6}\text{-}^tBu$, $(silox\text{-}d_9)_2(Me_3P)Mo{=}N^tBu$ ($\mathbf{6}\text{-}^tBu\text{-}d_{18}$), $(silox)_2(Me_3P)Mo{=}N^tAmyl$ ($\mathbf{6}\text{-}^tAmyl$), and $\mathbf{6}\text{-}^tAmyl\text{-}d_{18}$ (eq

$$\underset{\mathbf{6}\text{-}^tBu}{\mathbf{6}\text{-}^tBu} + \underset{\mathbf{6}\text{-}^tBu\text{-}d_{18}}{(silox\text{-}d_9)_2(Me_3P)Mo{=}N^tBu} + \underset{\mathbf{6}\text{-}^tAmyl}{(silox)_2(Me_3P)Mo{=}N^tAmyl} + \underset{\mathbf{6}\text{-}^tAmyl\text{-}d_{18}}{\mathbf{6}\text{-}^tAmyl\text{-}d_{18}} \quad (10)$$

10) The expected molecular ions from the possible exchanges are listed in Table 6.

Before the mass spectra of the crossover mixtures were obtained, it was necessary to optimize the experimental conditions, which was done using $\mathbf{6}\text{-}^tBu$. After an exhaustive solvent investigation, acetonitrile was discovered to yield satisfactory mass spectra, albeit with the PMe_3 replaced by two acetonitriles, that is, $(silox)_2Mo{=}N^tBu(NCCH_3)_2$ ($\mathbf{5}\text{-}^tBu\text{-}A_2$). The spectra revealed isotopic patterns (Mo^{92}, 14.8% abundance, 91.9063 amu; Mo^{94}, 9.3%, 93.9047 amu; Mo^{95}, 15.9%, 94.9058 amu; Mo^{96}, 16.7%, 95.9046 amu; Mo^{97}, 9.6%, 96.9058 amu; Mo^{98}, 24.1%, 97.9055 amu; and Mo^{100}, 9.6%, 99.9076 amu) consistent with $\mathbf{5}\text{-}^tBu\text{-}A_2$, $(silox)_2Mo{=}N^tBu(NCCH_3)$ ($\mathbf{5}\text{-}^tBu\text{-}A$) and $(silox)_2Mo{=}N^tBu$ ($\mathbf{5}\text{-}^tBu$). By lowering the cone voltage, conditions were determined whereby only $\mathbf{5}\text{-}^tBu\text{-}A_2$ was observed, and under these same conditions, $(silox)_2Mo{=}N^tAmyl(NCCH_3)_2$ ($\mathbf{5}\text{-}^tAmyl\text{-}A_2$) was also observed with an insignificant amount of side products.

Figure 13 illustrates the mass spectra of the necessary control experiments that show the acetonitrile matrix does not induce crossover. In the top spectrum, a mixture of $(silox)_2(Me_3P)Mo{=}N^tBu$ ($\mathbf{6}\text{-}^tBu$) and $(silox\text{-}d_9)_2(Me_3P)Mo{=}N^tAmyl$ ($\mathbf{6}\text{-}^tAmyl\text{-}d_{18}$) that was stirred for 3 min in pentane manifests only $(silox)_2Mo{=}N^tBu(NCCH_3)_2$ ($\mathbf{5}\text{-}^tBu\text{-}A_2$) and $(silox\text{-}d_9)_2Mo{=}N^tAmyl(NCCH_3)_2$ ($\mathbf{5}\text{-}^tAmyl\text{-}A_2$) upon ionization from the acetonitrile matrix. Note that the ^{t}Amyl derivative ionizes with greater facility, as the greater intensity of $\mathbf{5}\text{-}^tAmyl\text{-}A_2$ attests. In the middle spectrum, a similarly stirred (4 min) 1:1:1:1 pentane mixture of $\mathbf{6}\text{-}^tBu$, $(silox)_2Mo{=}N^tAmyl(PMe_3)$ ($\mathbf{6}\text{-}^tAmyl$), $(silox\text{-}d_9)_2Mo{=}N^tBu(NCCH_3)_2$ ($\mathbf{6}\text{-}^tBu\text{-}d_{18}$), and $\mathbf{6}\text{-}^tAmyl\text{-}d_{18}$ was converted to their *bis*-acetonitrile adducts upon phosphine loss when dissolved in the matrix. The mixture does not *appear* statistical because of the tendency for the ^{t}Amyl derivatives to ionize more readily. There is a distinct difference in the top and middle spectra, hence differentiation between the fragment exchange (termed dissociation/recombination in Table 6, eq 7) and imido exchange pathways (termed imido exchange in Table 6, eq 8) should be trivial unless silox exchange (Table 6) intervenes. Finally, in the bottom spectrum, a mixture of $[(silox)_2Mo{=}N^tBu]_2Hg$ ($(\mathbf{5}\text{-}^tBu)_2Hg$) and $[(silox\text{-}d_9)_2MoN^tAmyl]_2Hg$ ($(\mathbf{5}\text{-}^tAmyl)_2Hg\text{-}d_{36}$) was quenched with PMe_3 after 7 h of an induction period, and the mass spectrum of the corresponding *bis*-acetonitrile adducts reveals a small amount of indeterminate exchange, consistent with Figure 11.

The crossover experiments of $[(silox)_2Mo{=}N^tBu]_2Hg$ ($(\mathbf{5}\text{-}^tBu)_2Hg$) and $[(silox\text{-}d_9)_2MoN^tAmyl]_2Hg$ ($(\mathbf{5}\text{-}^tAmyl)_2Hg\text{-}d_{36}$) were performed in benzene solution and quenched at various intervals during the crossover process. Figure 14 illustrates mass spectra of the quenched crossover products after 20, 50, and 65% crossover. Surprisingly, the 20% crossover spectrum reveals substantial siloxide exchange as evidenced

Table 6. Central Molecular Ions Expected for Various Isotopologues of (silox)$_2$Mo═N^{t}Bu(NCCH$_3$)$_2$ (**5**-^{t}Bu-A$_2$) and (silox)$_2$Mo═N^{t}Amyl(NCCH$_3$)$_2$ (**5**-^{t}Amyl-A$_2$) Depending of Type of Exchange Process

dissociation/recombination

compound	M^+
(silox)$_2$Mo═NtBu(NCCH$_3$)$_2$ **5**-^{t}Bu-A$_2$	680.0
(silox−d_9)$_2$Mo═N^{t}Amyl(NCCH$_3$)$_2$ **5**-^{t}Amyl-A$_2$-d_{18}	712.2

imido exchange

compound	M^+
(silox)$_2$Mo═N^{t}Bu(NCCH$_3$)$_2$ **5**-^{t}Bu-A$_2$	680.0
(silox)$_2$Mo═NtAmyl(NCCH$_3$)$_2$ **5**-^{t}Amyl-A$_2$	694.1
(silox−d_9)$_2$Mo═NtBu(NCCH$_3$)$_2$ **5**-^{t}Bu-A$_2$-d_{18}	698.2
(silox−d_9)$_2$Mo═NtAmyl(NCCH$_3$)$_2$ **5**-^{t}Amyl-A$_2$-d_{18}	712.2

siloxide exchange

compound	M^+
(silox)$_2$Mo═NtBu(NCCH$_3$)$_2$ **5**-^{t}Bu-A$_2$	680.0
(silox-d_9)(silox)Mo═NtBu(NCCH$_3$)$_2$ **5**-^{t}Bu-A$_2$-d_9	689.1
(silox)$_2$Mo═N^{t}Amyl(NCCH$_3$)$_2$ **5**-^{t}Amyl-A$_2$	694.1
(silox−d_9)$_2$Mo═NtBu(NCCH$_3$)$_2$ **5**-^{t}Bu-A$_2$-d_{18}	698.2
(silox-d_9)(silox)Mo═NtAmyl(NCCH$_3$)$_2$ **5**-^{t}Amyl-A$_2$-d_9	703.1
(silox-d_9)$_2$Mo═NtAmyl(NCCH$_3$)$_2$ **5**-^{t}Amyl-A$_2$-d_{18}	712.2

by significant intensity around 690 and 703. In fact, one can make the case that silox exchange is swifter than imido exchange because the relative intensity of the 703 mass peak recedes into a more statistical looking pattern as the crossover

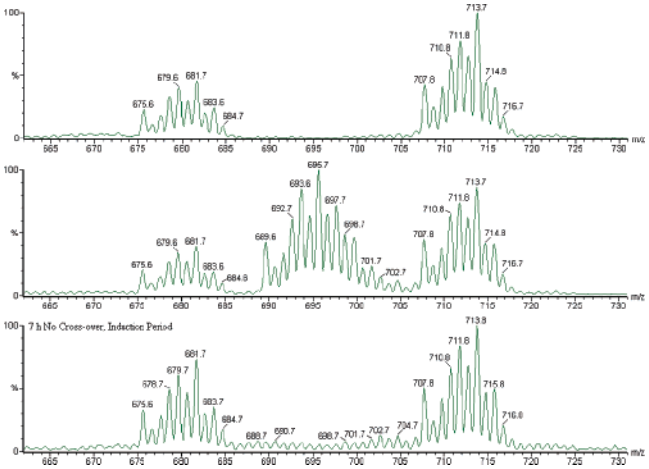

Figure 13. Mass spectral of control experiments featuring (top) a prepared 1:1 mixture of (silox)$_2$Mo═N^{t}Bu(PMe$_3$) (**6**-^{t}Bu) and of (silox-d_9)$_2$Mo═N^{t}Amyl(PMe$_3$) (**6**-^{t}Amyl-d_{18}) converted to (silox)$_2$Mo═N^{t}Bu(NCCH$_3$) (**5**-^{t}Bu-A$_2$) and (silox-d_9)$_2$Mo═N^{t}Amyl(NCCH$_3$)$_2$ (**5**-^{t}Amyl-A$_2$-d_{18}); (middle) a prepared 1:1:1:1 mixture of **6**-^{t}Bu, (silox)$_2$Mo═N^{t}Amyl(PMe$_3$) (**6**-^{t}Amyl), (silox-d_9)$_2$Mo═N^{t}Bu(NCCH$_3$)$_2$ (**6**-^{t}Bu-d_{18}), and **6**-^{t}Amyl-d_{18} converted to the *bis*-acetonitrile adducts via PMe$_3$ loss; and (bottom) crossover study of [(silox)$_2$Mo═N^{t}Bu]$_2$Hg ((**5**-^{t}Bu)$_2$Hg) and [(silox-d_9)$_2$MoN^{t}Amyl]$_2$Hg ((**5**-^{t}Amyl)$_2$Hg-d_{36}) quenched with PMe$_3$ while still during the induction period (7 h), and then converted to *bis*-acetonitrile adducts during preparation for mass spectral analysis.

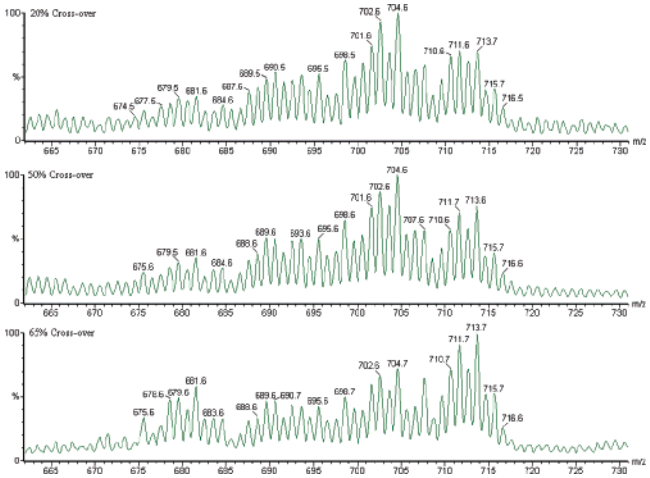

Figure 14. Mass spectra of experimental mixtures of of [(silox)$_2$Mo═N^{t}Bu]$_2$Hg ((**5**-^{t}Bu)$_2$Hg) and [(silox-d_9)$_2$MoN^{t}Amyl]$_2$Hg ((**5**-^{t}Amyl)$_2$Hg-d_{36}) quenched with PMe$_3$ (then exposed to MeCN for MS analysis) at 20 (top), 50 (middle), and 65% (bottom) conversion in the crossover region.

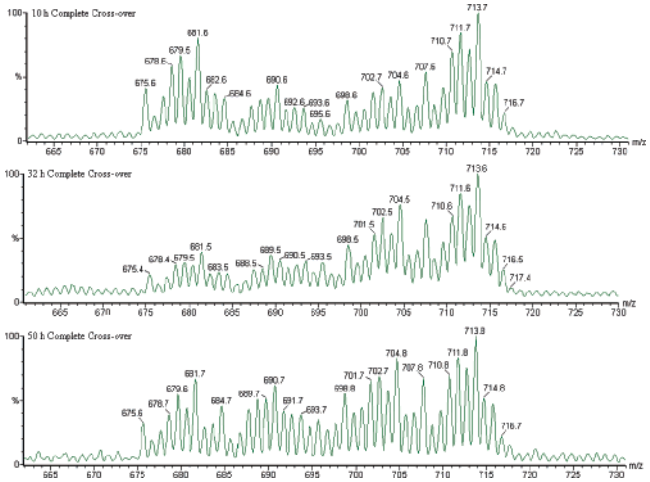

Figure 15. Mass spectra of experimental mixtures of of [(silox)$_2$Mo═N^{t}Bu]$_2$Hg ((**5**-^{t}Bu)$_2$Hg) and [(silox-d_9)$_2$MoN^{t}Amyl]$_2$Hg ((**5**-^{t}Amyl)$_2$Hg-d_{36}) quenched with PMe$_3$ (then exposed to MeCN for MS analysis) after complete crossover (10 h) and at 32 and 50 h after crossover.

progresses to 50 and 65%. Unfortunately this conclusion is tentative because once full crossover is achieved, as the 10, 32, and 50 h spectra in Figure 15 illustrate, subtle resolution differences can render their appearance quite different. There is no question, however, that silox exchange occurs readily, and this renders distinguishing the products from eqs 7 and 8 moot. The mechanism of crossover remains uncertain, but silox exchange as a critical step must be considered a strong possibility.

Discussion

Approaches toward (silox)$_2$Mo═NR. 1. Synthetic Studies. Although the synthetic target of this study, (silox)$_2$Mo═NR (**5**-R), has yet to be isolated, it is still a plausible intermediate in the chemistry of [(silox)$_2$Mo═NR]$_2$Hg (R = ^{t}Bu, (**5**-^{t}Bu)$_2$Hg; ^{t}Amyl, (**5**-^{t}Amyl)$_2$Hg), and in reductions of (silox)$_2$Cl$_2$Mo═NR (R = ^{t}Bu, (**1**-^{t}Bu); ^{t}Amyl, (**1**-^{t}Amyl) and (silox)$_2$ClMo═N^{t}Bu (**4**-^{t}Bu). Atom abstraction attempts to generate **5**-R also failed, and it appears that a bulkier R is necessary to prevent subsequent chemistry once **5**-R is

generated. Routes to **5**-Si^{t}Bu$_3$ and **5**-2,6-Ph$_2$-C$_6$H$_3$, for example, are now being sought.

2. Electronic Character of (silox)$_2$(X/L)$_n$Mo═NR. Electronic factors appear to govern the modest structural variations found in the class of Mo(IV) adducts (i.e., [(silox)$_2$Mo═N^{t}Bu]$_2$Hg ((**5**-^{t}Bu)$_2$Hg), (silox)$_2$(Me$_3$P)Mo═N^{t}Bu (**6**-^{t}Bu), and (silox)$_2$(4-pic)$_2$Mo═N^{t}Bu (**7**-4-pic)), and the Mo(V) chloride, (silox)$_2$ClMo═N^{t}Bu (**4**-^{t}Bu). The subtle pinching of the O−Mo−O angle versus the O−Mo−N angles in these derivatives provides greater stabilization of d_{yz} (π*(O)) vs d_{xz} (mostly (π*(N)), allowing the Mo(IV) species to possess diamagnetic character in cases of **6**-^{t}Bu and **7**-^{t}Bu. The best explanation for this general distortion is that it optimizes the π-donation from the better π-donor, the imide, in exchange for lesser π-bonding from the siloxides. In addition to this factor, **6**-^{t}Bu exhibits an unusual canting of the PMe$_3$ ligand. While this is easily construed as a subtle distortion to bring the P closer to the Mo for optimum π-backbonding, it is also plausible that a positional distortion of the phosphine provides some minimal σ/π-mixing that can strongly impact the strength of the Mo−P interaction.

It is difficult to argue that π-backbonding to the picoline ligands, which are not known to be effective π-acceptors, is a critical energetic cause of the modest distortions (silox)$_2$(4-pic)$_2$Mo═N^{t}Bu (**7**-4-pic)). In this case, the tipping of the picolines and the angular distortions aid in further maximizing π-donation from the imide. Furthermore, the slight distortion toward square pyramidal geometry attenuates the subtle *trans* influence of the picolines and permits some σ/π-mixing[9,10] to strengthen σ-interactions.

[(silox)$_2$Mo═NR]$_2$Hg (R = ^{t}Bu, (5-^{t}Bu)$_2$Hg; ^{t}Amyl, (5-^{t}Amyl)$_2$Hg): Nucleophilic Cleavage. The reactivity studies clearly point toward nucleophilic cleavage of [(silox)$_2$Mo═NR]$_2$Hg (R = ^{t}Bu, (**5**-^{t}Bu)$_2$Hg; ^{t}Amyl, (**5**-^{t}Amyl)$_2$Hg), as Scheme 3 indicates. Better nucleophiles, such as PMe$_3$ and py, immediately cleaved (**5**-^{t}Bu)$_2$Hg to give (silox)$_2$(PMe$_3$)Mo═N^{t}Bu (**6**-^{t}Bu) and (silox)$_2$(py)$_2$Mo═N^{t}Bu (**7**-py), and the former reaction was used in the analysis of the crossover studies. Poorer nucleophiles (e.g., ethylene, 2-butyne, N$_2$O, etc.) required longer reaction times to produce cleavage products, but the conditions were substantially less severe than those leading to degradation of (**5**-^{t}Bu)$_2$Hg. In addition, the extremely clean desulfurization of thiacrowns to yield (silox)$_2$(S)Mo═N^{t}Bu (**10**-^{t}Bu) and (silox)$_2$(C$_2$H$_4$)Mo═N^{t}Bu (**11**-^{t}Bu), which occurred over a lengthy time period at 23 °C, were nonetheless consistent with nucleophilic attack at Mo. A rapid, reversible Hg−Mo cleavage process could not be ruled out as a source of (silox)$_2$Mo═NR (**5**-R), which could subsequently be trapped by L, but the characteristics of the (**5**-R)$_2$Hg degradation process seem to put this possibility on a rather tenuous footing. Furthermore, additions of C$_2$H$_4$ and C$_2$Me$_2$ (in excess) to (silox)$_2$W═N^{t}Bu occur upon warming to 23 °C; if the crossover in eq 6 was occurring via free (silox)$_2$Mo═N^{t}Bu (**5**-^{t}Bu), trapping by excess C$_2$H$_4$ and C$_2$Me$_2$ would occur much swifter than observed. Recall that exposure of (silox)$_2$(Me$_3$P)Mo═N^{t}Bu (**6**-^{t}Bu) to C$_2$H$_4$ and C$_2$Me$_2$ afforded (silox)$_2$(C$_2$H$_4$)Mo═N^{t}Bu (**11**-^{t}Bu) and (silox)$_2$(C$_2$Me$_2$)Mo═N^{t}Bu (**8**-^{t}Bu) under mild conditions.

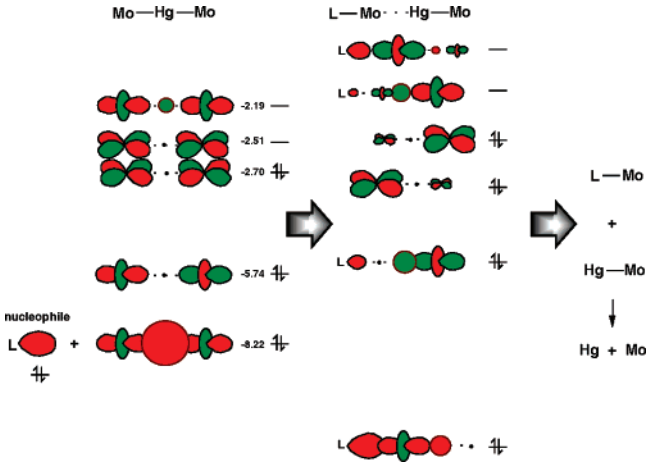

Figure 16. Simplified molecular orbital correlation of nucleophilic attack by L on [(silox)$_2$Mo═NR]$_2$Hg ((**5**-R)$_2$Hg, here shown as Mo−Hg−Mo) to give (silox)$_2$LMo═NR (L−Mo) and (silox)$_2$(Hg)Mo═NR (Hg−Mo) as initial products. Initial orbital energies (eV) are estimated from [(HO)$_2$Mo═NH]$_2$Hg (**5′**$_2$-Hg) in Figure 8.

The susceptibility of [(silox)$_2$Mo═NR]$_2$Hg (R = ^{t}Bu, (**5**-^{t}Bu)$_2$Hg; ^{t}Amyl, (**5**-^{t}Amyl)$_2$Hg) to attack by nucleophiles can be readily rationalized via the simplified molecular orbital correlation diagram illustrated in Figure 16. In (**5**-R)$_2$Hg, the two orbitals that constitute the 3c4e bond (one σ-bonding at −8.22 eV (and its lower energy partner) and one nonbonding at −5.74 eV)[19] are filled, while the wholly antibonding σ*-orbital at −2.19 eV is empty. The HOMO is the "stretched π-bonding" orbital at −2.70 eV. As the nucleophile L interacts with (**5**-R)$_2$Hg along *z*, two bonding MOs are created, one L−Mo bonding and the other Hg−Mo bonding, along with their corresponding antibonding MOs. The additional electrons are deposited in the stretched π*-orbital, and cleavage leads to (silox)$_2$(L)Mo═NR (L−Mo) and (silox)$_2$(Hg)Mo═NR (Hg−Mo) adducts that each have two π-type electrons and two electrons in their respective adduct bonding orbital. In effect, the low-lying stretched π-type orbitals serve as a reservoir for the additional electron density added by the incoming L, and this process is facilitated by σ/π-mixing. Cleavage by L of the 3c4e bond is a logical consequence of its composition; one bonding and one nonbonding orbital are converted into two σ-bonds, the strong Mo−L and the weak Mo−Hg.

Thermal Stability of [(silox)$_2$Mo═NR]$_2$Hg: Consequences of Orbital Symmetry. The experiments regarding the thermal stability and degradation mechanism of [(silox)$_2$Mo═NR]$_2$Hg (R = ^{t}Bu, (**5**-^{t}Bu)$_2$Hg; ^{t}Amyl, (**5**-^{t}Amyl)$_2$Hg) were predicated on the basis of calculations pertaining to the model [(HO)$_2$Mo═NH]$_2$Hg (**5′**$_2$-Hg). These calculations were difficult, and their veracity is difficult to discern with great confidence without greater experimentation. Nonetheless, the striking difference between the calculated *D*(MoHg) and the apparent dissociation or degradation rate was believed to be outside reasonable bounds of calculational error given previous experience.

On the basis of the calculated bond dissociation enthalpy (~23 kcal/mol) for the Mo−Hg bond in [(silox)$_2$Mo═

NR]$_2$Hg (R = ^{t}Bu, (**5**-^{t}Bu)$_2$Hg; ^{t}Amyl, (**5**-^{t}Amyl)$_2$Hg), the dissociation to 2 **5**-R + Hg was predicted to be swift. The tremendous stability accorded the trinuclear species stems from the forbidden orbital symmetry of the dissociation process. One simple description of the ground state electronic configuration of (**5**-R)$_2$Hg is $\sigma^2\sigma^2\pi^2$, which shows the type and occupancy of the orbitals critical to Mo−Hg and Mo···Mo bonding ($2a_g$, $1b_u$, and $2a_u$ in Figure 8). The orbital symmetries of the dissociation products (silox)$_2$Mo═NR (**5**-R) and (silox)$_2$(Hg)Mo═NR (**5**-R-Hg) are π^2 and $\sigma^2\pi^2$, respectively, and the dissociation is orbitally forbidden because it is a $\sigma^2\sigma^2\pi^2 \rightarrow \pi^2 + \sigma^2\pi^2$ process. Note that this path is predicted to have a higher dissociation barrier *on the basis of orbital symmetry arguments alone; spin changes are not consequential*. In accord with experiment, the calculated crossing point for dissociation is substantially higher than that predicted by the *D*(Mo−Hg), and it is in reasonable agreement with the phenomenological degradation rate.

2. Mechanism of Label Crossover. The erratic nature of the degradation of [(silox)$_2$Mo═NR]$_2$Hg (R = ^{t}Bu, (**5**-^{t}Bu)$_2$Hg; ^{t}Amyl, (**5**-^{t}Amyl)$_2$Hg), especially with regard to the crossover studies, prevents a conclusive answer to the mechanism of degradation. A rough interpretation of the data in Table 6 permits a reasonable mechanism to be proposed, although it must remain tentative. The induction period for crossover is about the same as the original degradation rate assessed for (**5**-^{t}Bu)$_2$Hg, and while this observation could imply reversibility of Mo−Hg dissociation, this is unlikely in view of the more pronounced crossover rates within the "crossover region". Within the crossover region, the data, with the exception of run 6, is best fit to a phenomenological rate expression that is 3/2-order in [(**5**-^{t}Bu)$_2$Hg]. A plausible

$$\underset{(\mathbf{5}\text{-}^t\mathrm{Bu})_2\mathrm{Hg}}{[(\mathrm{silox})_2\mathrm{Mo}{=}\mathrm{N}^t\mathrm{Bu}]_2\mathrm{Hg}} \xrightarrow{k_{diss}} \mathrm{Hg} + 2\ \underset{\mathbf{5}\text{-}^t\mathrm{Bu}}{(\mathrm{silox})_2\mathrm{Mo}{=}\mathrm{N}^t\mathrm{Bu}} \quad (11)$$

$$\mathbf{5}\text{-}^t\mathrm{Bu} \xrightarrow{k_{deg}} \text{degradation} \quad (12)$$

$$\mathbf{5}\text{-}^t\mathrm{Bu} + \underset{(\mathbf{5}\text{-}^t\mathrm{Amyl})_2\mathrm{Hg}}{[(\mathrm{silox})_2\mathrm{Mo}{=}\mathrm{N}^t\mathrm{Amyl}]_2\mathrm{Hg}} \xrightarrow{k_{xovr}} \underset{\mathbf{5}\text{-}^t\mathrm{Amyl}}{(\mathrm{silox})_2\mathrm{Mo}{=}\mathrm{N}^t\mathrm{Amyl}} + \underset{(\mathbf{5}\text{-}^t\mathrm{Bu})\mathrm{Hg}(\mathbf{5}\text{-}^t\mathrm{Amyl})}{[(\mathrm{silox})_2\mathrm{Mo}{=}\mathrm{N}^t\mathrm{Amyl}]\mathrm{Hg}[(\mathrm{silox})_2\mathrm{Mo}{=}\mathrm{N}^t\mathrm{Bu}]} \quad (13)$$

mechanism is given in eqs 11−13; a parallel set of equations exists for (**5**-^{t}Amyl)$_2$Hg. (**5**-^{t}Bu)$_2$Hg undergoes a slow, irreversible degradation to give (silox)$_2$Mo═N^{t}Bu (**5**-^{t}Bu, eq 11). The monomer can degrade in a first-order fashion (eq 12)u or react with an intact (**5**-^{t}Amyl)$_2$Hg molecule in a second-order exchange (eq 13, presumably an imido or silox exchange) process. Under the right circumstances, the first-order degradation in eq 12 might be swift, yet allow [**5**-^{t}Bu] to slowly build up until the second-order exchange process, which does not consume **5**-^{t}Bu (or **5**-^{t}Amyl), becomes competitive with the degradation.

The problem with this mechanism is that the irreversible k_{diss} path shown in eq 11 would provide **5**-^{t}Bu in a *first-order* process, hence leading to an overall second-order exchange path (eq 13). It is interesting to note that Schrock has prepared a number of Mo and W compounds of the sort [(X)(Y)M═NR]$_2$ that contain M═M bonds.[38−41] If the steady-state concentration of **5**-^{t}Bu (and **5**-^{t}Amyl) is stabilized by dimerization, such as that shown in eq 14, then its concentration would be half-order in [(**5**-^{t}Bu)$_2$] (or [**5**-^{t}Amyl]$_2$

$$\underset{(\mathbf{5}\text{-}^t\mathrm{Bu})_2}{[(\mathrm{silox})_2\mathrm{Mo}{=}\mathrm{N}^t\mathrm{Bu}]_2} \underset{k_d}{\overset{k_m}{\rightleftharpoons}} 2\ \underset{\mathbf{5}\text{-}^t\mathrm{Bu}}{(\mathrm{silox})_2\mathrm{Mo}{=}\mathrm{N}^t\mathrm{Bu}} \quad (14)$$

and [(**5**-^{t}Bu)(**5**-^{t}Amyl)]), which is derived from a first-order degradation of the starting mercury complex. As a consequence, the degradation in eq 12 would similarly be half-order, and the exchange process in eq 13 would be overall 3/2 order in starting complex. This would suggest the induction period for ligand exchange would be inversely proportional to starting concentration. As Table 6 shows, while this seems to be the case for runs 1−4, runs 5 and 6 illustrate the erratic behavior that renders interpretation of the induction period difficult.

It is also possible that eq 11 is reversible enough that [(**5**-^{t}Bu)$_2$] would be half-order in [(**5**-^{t}Bu)$_2$Hg] and eq 13 would not be competitive with eq 12 until sufficient **5**-^{t}Bu was generated. In this instance, note that reversible Mo−Hg bond formation is not enough to explain the ligand exchanges observed by mass spectrometry, which require a mechanism independent from simple dissociation. The crossover region manifests the process represented by eq 13. It is conceivable that impurities such as M(silox) (e.g., M = Na) or H(silox) could mediate certain exchanges, but it is difficult to reconcile the induction periods in such cases.

Experimental Section

General Considerations. All manipulations of air-sensitive materials were performed using glove box and high-vacuum techniques under an inert atmosphere. Hydrocarbon or ethereal solvents were refluxed over sodium and vacuum transferred from sodium benzophenone ketyl (with 3−6 mL of tetraglyme/L added to hydrocarbons). Benzene-d_6 was sequentially dried over sodium and then 4 Å molecular sieves and vacuum transferred from the 4 Å molecular sieves. All glassware was oven dried for a minimum of 4 h. NMR tubes for sealed-tube experiments and glass bombs were flame dried under dynamic vacuum prior to use. (DME)Cl$_2$Mo(═N^{t}Bu)$_2$ (**1**-^{t}Bu),[20−22] Ti{N(SiMe$_3$)$_2$}$_3$,[34] and ^{t}BuLi-d_9[42] were prepared according to literature procedures.

^{1}H, ^{13}C{^{1}H}, ^{13}C, and ^{31}P{^{1}H} NMR spectra were obtained on Varian Mercury 300, XL-400, and Unity 500 spectrometers. Chemical shifts are reported relative to benzene-d_6 (^{1}H, δ 7.15; ^{13}C, δ 128.00) and phosphoric acid (^{31}P, δ 0.00). Infrared spectra were recorded using a Nicolet Impact 410 spectrophotometer interfaced to an IBM PC. Mass spectra were obtained on a Fisions Instruments VG Quattro electrospray ionization mass spectrometer

(42) Bailey, W. F.; Nurmi, T. T.; Patricia, J. J.; Wang, W. *J. Am. Chem. Soc.* **1987**, *109*, 2442−2448.

interfaced with an IBM PC. Combustion analyses were performed by Oneida Research Services, Whitesboro, NY, or Robertson Microlit Laboratories, Madison, NJ.

Procedures. 1. (DME)Cl_2Mo(=NCEt(Me)$_2$)$_2$ (1-^{t}Amyl). A 50 mL round-bottom flask connected to a reflux condenser was charged with K_2MoO_4 (1.023 g, 4.29 mmol). The apparatus was evacuated, and 20 mL of dimethoxyethane was added via vacuum transfer at −78 °C. Triethylamine (2.40 mL, 17.2 mmol), chlorotrimethylsilane (4.79 mL, 38.61 mmol), and *tert*-amylamine (1.00 mL, 8.59 mmol) were sequentially added via vacuum transfer at −78 °C from a volumetric finger. The reaction mixture was allowed to slowly warm to 25 °C and was heated with stirring at 70 °C for 16 h. After the reaction mixture cooled to 25 °C, it was filtered away from the white precipitate to yield a yellow liquid. The solvent was removed in vacuo with the resulting yellow solid recrystallized from 10 mL of diethyl ether to yield 1.426 g **1**-^{t}Amyl (77%). ^{1}H NMR (benzene-d_6): δ 1.08 (t, J = 7 Hz, 6H, CH_2CH_3), 1.42 (s,12H, CCH_3), 1.73 (q, J = 7 Hz, 4H, CH_2CH_3), 3.21 (s, 4H, OCH_2), 3.46 (s, 6H, OCH_3). ^{13}C NMR (benzene-d_6): δ 9.53 (q, J = 125 Hz, CH_2CH_3), 27.82 (q, J = 123 Hz, $C(CH_3)_2CH_2CH_3$), 36. 98 (t, J = 129 Hz, $C(CH_3)_2CH_2CH_3$), 62.60 (q, J = 144 Hz, OCH_3), 70.70 (t, J = 146, OCH_2), 75.00 (s, $C(CH_3)_2CH_2CH_3$). IR (Nujol mull, NaCl, cm^{-1}): 1328 (m), 1288 (s), 1202 (s), 1120 (s), 1043 (s), 910 (m), 870 (s), 830 (s), 771 (s), 612 (m), 599 (s). Anal. Calcd $C_{14}H_{32}N_2O_2Cl_2Mo$: C, 39.30; H, 7.55; N, 6.56. Found: C, 38.13; H, 7.34; N, 6.51.

2. (silox)$_2$Mo(=N^{t}Bu)$_2$ (2-^{t}Bu). To a 25 mL flask containing (DME)Cl_2Mo(=N^{t}Bu)$_2$ (**1**-^{t}Bu) (0.415 g, 1.04 mmol) and ^{t}Bu$_3$SiONa (0.495 g, 2.08 mol) was distilled 12 mL THF at −78 °C. The solution was stirred at 23 °C for 12 h. The volatiles were removed in vacuo, and the residue was triturated with hexanes (3 × 10 mL). The reaction was filtered using hexanes (15 mL), and the filtrate volume was reduced to 6 mL and cooled to −78 °C. Filtration yielded 0.376 g of **2**-^{t}Bu as a white solid (54%). IR (Nujol Mull, NaCl, cm^{-1}): 1354 (s), 1255 (s), 1216 (m), 1003 (m), 964 (s), 904 (s), 818 (s), 619 (s). Anal. Calcd $C_{32}H_{72}N_2O_2Si_2Mo$: C, 57.45; H, 10.85; N, 4.19. Found: C, 57.52; H, 11.14; N, 4.05.

3. (silox)$_2$Cl$_2$Mo=N^{t}Bu (3-^{t}Bu). A glass bomb reactor was charged with (DME)Cl_2Mo(=N^{t}Bu)$_2$ (**1**-^{t}Bu) (5.018 g, 12.57 mmol) and ^{t}Bu$_3$SiOH (5.430 g, 25.14 mmol). The system was evacuated, and 25 mL of benzene was vacuum transferred at −78 °C. One equiv of HCl (12.57 mmol) was condensed via a calibrated gas bulb (308.8 mL) at 77 K. The mixture was allowed to slowly warm to 23 °C and was heated at 100 °C with stirring for 16−20 h. After the mixture had cooled to 23 °C, the volatiles were removed in vacuo, and the resulting orange/red solid was transferred to a flask using 25 mL of pentane. The mixture was triturated twice with 15 mL of pentane and filtered to remove the salt; the salt cake was washed with pentane until no orange material remained. The mixture was reduced to 8 mL, cooled to −78 °C for 20 min, and filtered to provide 6.90 g **3**-^{t}Bu (82% yield). IR (Nujol Mull, NaCl, cm^{-1}): 1387 (s), 1361 (s), 1222 (s), 1162 (w), 1040 (m), 1009 (w), 910 (s), 850 (s), 811 (s), 625 (s), 585 (w). Anal. Calcd $C_{28}H_{63}NO_2Si_2Cl_2Mo$: C, 50.28; H, 9.49; N, 2.09. Found: C, 50.16; H, 9.49; N, 2.04.

4. (silox)$_2$Cl$_2$Mo=NCEt(Me)$_2$ (3-^{t}Amyl). To a glass bomb reactor containing (DME)Cl_2Mo(=N-CEt(Me)$_2$)$_2$ (**1**, ^{t}Amyl) (2.010 g, 4.705 mmol) and ^{t}Bu$_3$SiOH (2.037 g, 9.410 mmol) was distilled 30 mL of benzene at −78 °C. One equiv of HCl (4.71 mmol) was admitted via a calibrated gas bulb (308.8 mL) at 77 K. The mixture was allowed to slowly warm to 25 °C and was heated with stirring at 100 °C for 16−20 h. Upon cooling to 23 °C, the volatiles were removed in vacuo leaving an orange/red residue. The residue was transferred into a 50 mL round-bottom flask using pentane (~25 mL). The mixture was triturated twice with 15 mL of pentane and filtered to remove the salt, and the salt cake was washed with pentane until no orange color remained. The mixture was reduced to 8 mL, cooled to −78 °C for 25 min, and filtered to yield **3**-^{t}Amyl as an orange/red solid (2.403 g, 75% yield). IR (Nujol mull, NaCl, cm^{-1}): 1381 (s), 1361 (s), 1288 (s), 1208 (s), 1062 (w), 1020 (m), 1009 (m), 910 (s), 840 (s), 811 (s), 618 (s), 592 (m), 519 (w). Anal. Calcd $C_{28}H_{63}NO_2Si_2Cl_2Mo$: C, 51.00; H, 9.59; N, 2.05. Found: C, 50.96; H, 9.79; N, 2.06.

5. (silox)$_2$(Cl)Mo=N^{t}Bu (4-^{t}Bu). To a 25 mL flask charged with (silox)$_2$$Cl_2$Mo=N^{t}Bu (**3**-^{t}Bu) (0.513 g, 0.767 mmol) and 0.95% Na/Hg (1.10 equiv, 2.100 g, 0.868 mmol) was distilled 10 mL diethyl ether. The solution warmed to 23 °C with stirring and became purple within 2 h. After 12 h, the volatiles were removed in vacuo, leaving a purple residue. Trituration with pentane (2 × 8 mL) was followed by filtration (5 mL), and the salt cake was washed until it was no longer purple. The filtrate volume was reduced to 2 mL, cooled to −78 °C for 40 min, and filtered to yield 0.282 g of **4**-^{t}Bu as a purple crystalline solid (58%). IR (Nujol mull, NaCl, cm^{-1}): 1369 (m), 1227 (m), 959 (s), 867 (s), 817 (s), 626 (s). Anal. Calcd $C_{28}H_{63}NO_2ClSi_2Mo$: C, 53.10; H, 10.03; N, 2.21. Found: C, 53.43; H, 9.85; N, 2.16. μ_{eff}(293 K) = 1.65 μ_B (Evans' method in C_6D_6).[23]

6. [(silox)$_2$Mo=NR]$_2$Hg ((5-R)$_2$Hg). a. (5-^{t}Bu)$_2$Hg. To a 25 mL flask containing (silox)$_2$$Cl_2$Mo=N^{t}Bu (**3**-^{t}Bu) (0.351 g, 0.525 mmol) and 0.95% Na/Hg (2.667 g, 1.102 mmol) was distilled 15 mL of diethyl ether. The solution slowly warmed to 23 °C, accompanied by stirring, and after 1 h the mixture had become green/brown in color. After 17 h of stirring, the solvent was removed in vacuo leaving a green/brown residue. The Hg^0 was decanted away, and the mixture was triturated with pentane (2 × 10 mL) and filtered to remove salt and remaining Hg^0. The solvent volume was reduced to 3 mL, and the mixture was cooled to −78 °C for 2 h. Filtration left an olive green solid, which was washed once with 2 mL of cold pentane to yield 0.204 g of (**5**-^{t}Bu)$_2$Hg (56%). IR (Nujol mull, NaCl, cm^{-1}): 1381 (s), 1361 (s), 1235 (m), 1210 (m), 1016 (w), 930 (s), 883 (s), 811 (s), 625 (s). Anal. Calcd $H_{126}C_{56}Si_4O_4N_2Mo_2Hg$: C, 48.16; H, 9.09; N, 2.00. Found: C, 47.95; H, 9.33; N, 1.92. μ_{eff}(293 K) = 1.15 μ_B (Evans' method in C_6D_6).[23]

b. (5-^{t}Amyl)$_2$Hg. (5-^{t}Amyl)$_2$Hg was prepared using the same protocol as in a. **3**-^{t}Amyl (0.385 g, 0.565 mmol) and 0.95% Na/Hg (2.969 g, 1.186 mmol) yielded (**5**-^{t}Amyl)$_2$Hg (0.156 g, 39%). IR (Nujol mull, NaCl, cm^{-1}): 1388 (s), 1361 (m), 1288 (w), 1229 (m), 1210 (w), 1016 (w), 930 (s), 884 (s), 818 (s), 632 (s). Anal. Calcd $C_{58}H_{130}N_2O_4Si_4Mo_2Hg$: C, 48.90; H, 9.20; N, 1.97. Found: C, 48.54; H, 9.20; N, 1.87.

7. (silox)$_2$(Me$_3$P)Mo=NR (6-R). a. 6-^{t}Bu. To a 25 mL flask containing (silox)$_2$$Cl_2$Mo=N^{t}Bu (**3**-^{t}Bu, 0.658 g, 0.984 mmol) and 0.95% Na/Hg (2.10 equiv, 5.00 g, 2.07 mmol) was distilled 10 mL PMe_3 at −78 °C. The reaction mixture warmed to 23 °C with stirring and became brown/red in color within 1 h. The mixture was stirred for 12 h and changed color from red/brown to maroon. All volatiles were removed in vacuo, and the maroon residue was triturated with pentane (5 × 10 mL). The reaction mixture was filtered using pentane to remove Hg^0 and salt and was washed until all red color was removed from the salt cake. The solvent was then removed from the mixture to yield 0.505 g of **6**-^{t}Bu as a maroon solid (76%). IR (Nujol mull, NaCl, cm^{-1}): 1480 (s), 1381 (m), 1355 (w), 1282 (w), 1249 (s), 1215 (w), 970 (s), 930 (s), 884 (s), 818 (s), 738 (w), 665 (w), 619 (s). Anal. Calcd $C_{31}H_{72}NO_2Si_2PMo$: C, 55.24; H, 10.77; N, 2.08. Found: C, 55.29; H, 10.90; N, 1.74.

b. 6-^{t}Amyl. Prepared via the protocol in a; (silox)$_2$Cl$_2$Mo=NCEt(Me)$_2$ (**3**-^{t}Amyl, 0.402 g, 0.590 mmol) and 0.95% Na/Hg (2.996 g, 1.238 mmol) yielded **6**-^{t}Amyl (0.239 g, 59%). IR (Nujol mull, NaCl, cm^{-1}): 1480 (s), 1381 (m), 1295 (w), 1229 (m), 1010 (w), 964 (s), 930 (s), 884 (s), 818 (s), 665 (w), 625 (s). Anal. Calcd $C_{32}H_{74}NO_2Si_2PMo$: C, 55.86; H, 10.84; N, 2.04. Found: C, 55.59; H, 10.61; N, 1.95.

8. (silox)$_2$(py)$_2$Mo=N^{t}Bu (7-py). a. From Na/Hg. To a 25 mL flask charged with (silox)$_2$Cl$_2$Mo=N^{t}Bu (**3**-^{t}Bu) (0.789 g, 1.180 mmol) and 0.95% Na/Hg (6.002 g, 2.480 mmol) was vacuum transferred 12 mL pyridine at −78 °C. The mixture was warmed to room temperature (RT) with stirring and became navy blue/purple in color within 1 h. Stirring continued for 12 h, and the pyridine was removed in vacuo. The residue was triturated with pentane (5 × 5 mL) and filtered until no blue color remained on the filter cake. The blue/purple solution was reduced in volume to 3 mL, cooled to −78 °C for 2 h, and filtered to yield **7**-py (0.534 g, 60%) as dark blue crystals.

b. From K/C$_8$. Into a flask containing **3**-^{t}Bu (0.190 g, 0.284 mmol) and K/C$_8$ (2.20 equiv, 0.085 g, 0.625 mmol) was distilled 4 mL pyridine at −78 °C. The solution was warmed to 0 °C with stirring, and it became dark blue in ∼20 min. After the mixture was stirred for 1 h at 0 °C, the solvent was removed in vacuo, and the resulting dark blue residue was triturated with hexanes (5 × 4 mL). The mixture was filtered using hexanes and washed until there was no blue color left on the salt cake, yielding a dark blue solution. Reduction of the solution volume to 2 mL, cooling to −78 °C for 30 min, and filtration yielded 0.101 g of **7**-py(47%). IR (Nujol Mull, NaCl, cm^{-1}): 1580 (s), 1546 (m), 1481 (s), 1381 (s), 1361 (s), 1235 (s), 1215 (m), 1202 (s), 1043 (w), 1003 (m), 977 (s), 910 (s), 817 (s), 751 (s), 678 (s), 612 (m). Anal. Calcd $C_{38}H_{73}N_3O_2Si_2Mo$: C, 60.36; H, 9.73; N, 5.56. Found: C, 59.72; H, 9.72; N, 4.81.

9. (silox)$_2$(4-pic)$_2$Mo=N^{t}Bu (7-4-pic). To a 10 mL flask containing (silox)$_2$Cl$_2$Mo=N^{t}Bu (**3**-^{t}Bu, 0.245 g, 0.366 mmol) and 0.95% Na/Hg (1.861 g, 0.769 mmol) was distilled 5 mL of 4-picoline at −78 °C. The reaction mixture was warmed to 25 °C and became navy blue/purple in color within 1 h. After 4 h, the 4-picoline was removed in vacuo, and the resulting blue/purple solid was triturated with pentane (5 × 5 mL). The mixture was filtered (6 mL pentane) and washed to remove Hg° and salts. The resulting blue/purple solution was reduced in volume to 3 mL, cooled to −78 °C for 20 min, and filtered to yield dark blue/black crystals of **7**-4-pic (58%). IR (Nujol mull, NaCl, cm^{-1}): 1607 (m), 1534 (w), 1480 (s), 1361 (m), 1235 (s), 1043 (w), 990 (s), 917 (s), 818 (m), 806 (m), 619 (s). Anal. Calcd $C_{40}H_{77}N_3O_2Si_2Mo$: C, 61.26; H, 9.89; N, 5.36. Found: C, 58.10; H, 9.92; N, 3.98.

10. (silox)$_2$Mo=N^{t}Bu(C$_2$Me$_2$) (8-^{t}Bu). To a 10 mL flask charged with (silox)$_2$(Me$_3$P)Mo=N^{t}Bu (**6**-^{t}Bu, 0.248 g, 0.368 mmol) was added pentane (5 mL) via vacuum transfer at −78 °C. Five equivalents of 2-butyne (1.84 mmol) was added through a calibrated gas bulb. The solution was warmed to 23 °C with stirring. After 6 h, it became yellow in color, and removal of the volatiles in vacuo yielded a dark yellow solid. The solid was triturated with pentane (2 × 4 mL), and the solvent volume reduced was to 2 mL. The mixture was filtered to yield 0.168 g **8**-^{t}Bu (67%). IR (Nujol mull, NaCl, cm^{-1}): 1481 (s), 1388 (s), 1361 (m), 1242 (s), 1215 (w), 1149 (w), 1017 (w), 957 (s), 884 (s), 818 (s), 625 (s). Anal. Calcd $C_{32}H_{69}NO_2Si_2Mo$: C, 58.95; H, 10.67; N, 2.15. Found: C, 58.93; H, 10.61; N, 2.08.

11. (silox)$_2$(O)Mo=N^{t}Bu (9-^{t}Bu). To a 25 mL flask charged with (silox)$_2$(py)$_2$Mo=N^{t}Bu (**7**-py, 0.248 g, 0.327 mmol) was vacuum transferred benzene (10 mL) at −78 °C. N_2O (1.5 equiv, 0.491 mmol) was admitted via a calibrated gas bulb (109.4 mL), and the solution was warmed to 23 °C with stirring. After ∼5 min at 23 °C, effervescence occurred (N_2 release), and the color became light brown. After the mixture was stirred for 2 h, the volatiles were removed in vacuo, leaving a light brown residue that was triturated with hexanes (3 × 8 mL). The light brown solid was dissolved in 3 mL of pentane, and slow evaporation at −35 °C yielded **9**-^{t}Bu (0.171 g, 85%) as a crystalline white solid. IR (Nujol mull, NaCl, cm^{-1}): 1480 (m), 1387 (m), 1361 (w), 1222 (m), 1010 (w), 970 (s), 930 (s), 897 (s), 818 (s), 625 (s). Anal. Calcd $C_{28}H_{63}NO_3Si_2Mo$: C, 54.78; H, 10.34; N, 2.28. Found C: 55.00; H, 10.40; N, 2.11.

12. (silox)$_2$(S)Mo=N^{t}Bu (10-^{t}Bu). To a 25 mL flask charged with [(silox)$_2$Mo=N^{t}Bu]$_2$Hg (**5**-^{t}Bu)$_2$Hg, 0.278 g, 0.199 mmol) and S_8 (1 equiv, 0.052 g, 0.200 mmol) was distilled 12 mL benzene. The solution was stirred for 12 h at 23 °C, and a black precipitate was generated. The volatiles were removed in vacuo leaving an olive green residue. The solids were triturated with pentane (3 × 10 mL), and the mixture was filtered to give a yellow solution. The filter cake was washed with pentane until it was no longer yellow. The solvent was removed and the canary yellow solid was dried 12 h under dynamic vacuum to yield 0.220 g of **10** (88%). IR (Nujol mull, NaCl, cm^{-1}): 1388 (m), 1361 (m), 1215 (s), 1017-(w), 957 (s), 937 (s), 897 (s), 818 (s), 725 (w), 625 (s). Anal. Calcd $C_{28}H_{63}NO_2Si_2SMo$: C, 53.38; H, 10.08; N, 2.22. Found: C, 52.43; H, 9.93; N, 1.98.

13. (silox)$_2$(C$_2$H$_4$)Mo=N^{t}Bu (11-^{t}Bu). To a 10 mL flask charged with (silox)$_2$(Me$_3$P)Mo=N^{t}Bu (**6**-^{t}Bu, 0.262 g, 0.389 mmol) was vacuum transferred 6 mL of pentane at −78 °C. Ethylene (420 Torr) was admitted via a calibrated gas bulb, and the solution was warmed to 23 °C. After ∼20 min, the solution became pink/purple and was stirred for 3 h. The volatiles were removed in vacuo yielding a pink/purple solid. The residue was triturated using pentane (4 × 5 mL). The solution was reduced to 3 mL, cooled to −78 °C for 2 h, and filtered to yield 0.174 g of **11**-^{t}Bu as a pink/purple solid (72%). IR (Nujol mull, NaCl, cm^{-1}): 3051 (w), 1481 (s), 1388 (m), 1361 (m), 1249 (s), 1215 (w), 1136 (m), 1010 (w), 964 (s), 884 (s), 824 (s), 738 (m), 625 (s). Anal. Calcd $C_{30}H_{67}NO_2Si_2Mo$: C, 57.56; H, 10.79; N, 2.24. Found: C, 57.82; H, 10.91; N, 2.19.

NMR Tube Reactions. General. Flame-dried NMR tubes, sealed onto 14/20 ground glass joints, were charged with metal reagent (typically 20 mg, ∼1 × 10^{-5} mol) in the dry box and moved to the vacuum line on needle valve adapters. The NMR tubes were degassed, and after transfer of deuterated solvent, a calibrated gas bulb was used to introduce volatile reagents at 77 K. The tubes were sealed with a torch. Solid substrates were loaded along with the metal complex followed by solvent transfer on the vacuum line and flame sealing. Freshly distilled deuterated solvent was added to NMR tubes containing substrate and metal complex while in the dry box. The mixture was then degassed on the vacuum line, and the tube was flame sealed. Reactions were monitored by ^{1}H NMR spectroscopy unless noted.

14. [(silox)$_2$Mo=N^{t}Bu]$_2$Hg ((5-^{t}Bu)$_2$Hg) + excess pyridine. To an NMR tube containing (**5**-^{t}Bu)$_2$Hg (0.028 g, 2.0 × 10^{-2} mmol) was distilled in C_6D_6 and ∼0.1 mL of pyridine at 77 K. When warmed to 23 °C, the solution became dark blue, and the analysis revealed 93% conversion to **7**-py and excess pyridine.

15. [(silox)$_2$Mo=N^{t}Bu]$_2$Hg ((5-^{t}Bu)$_2$Hg) and xs 2,6-lutidine. To an NMR tube containing (**5**-^{t}Bu)$_2$Hg (0.026 g, 1.9×10^{-2} mmol) was transferred C_6D_6, and 2,6-lutidine.

16. [(silox)$_2$Mo=N^{t}Bu]$_2$Hg ((5-^{t}Bu)$_2$Hg) and 4.7 PMe$_3$. To an NMR tube containing (**5**-^{t}Bu)$_2$Hg (0.031 g, 2.2×10^{-2} mmol) was transferred C_6D_6, and PMe_3 (0.104 mmol) via a calibrated gas bulb. When the tube was warmed to 23 °C, the solution became maroon, and the analysis revealed full conversion to **6**-^{t}Bu and Hg°.

17. [(silox)$_2$Mo=N^{t}Bu]$_2$Hg ((5-^{t}Bu)$_2$Hg) and 4.8 2-butyne. To an NMR tube containing (**5**-^{t}Bu)$_2$Hg (0.026 g, 1.86×10^{-2} mmol) was distilled in C_6D_6, and 4.8 equiv 2-butyne (9.30×10^{-2} mmol) was admitted via a calibrated gas bulb. After 27 days at 23 °C, followed by 45 h at 70 °C, full conversion to (silox)$_2$Mo=N^{t}Bu(C_2Me_2) (**8**-^{t}Bu) was noted.

18. [(silox)$_2$Mo=N^{t}Bu]$_2$Hg ((5-^{t}Bu)$_2$Hg) and 2.20 N$_2$O. To an NMR tube charged with (**5**-^{t}Bu)$_2$Hg (0.031 g, 0.022 mmol) dissolved in C_6D_6 was admitted 2.20 equiv N_2O via a calibrated gas bulb. After 16 h at 23 °C, 10% conversion to (^{t}Bu$_3$SiO)$_2$(O)Mo=N^{t}Bu (**9**-^{t}Bu) was observed, and full conversion occurred after 20 h at 60 °C.

19. [(silox)$_2$Mo=N^{t}Bu]$_2$Hg ((5-^{t}Bu)$_2$Hg) and 400 Torr of H$_2$. To an NMR tube charged with (**5**-^{t}Bu)$_2$Hg was distilled C_6D_6 followed by 400 torr H_2. No reaction was observed after a substantial period at 25 °C and thermolysis at 100 °C.

20. [(silox)$_2$Mo=N^{t}Bu]$_2$Hg ((5-^{t}Bu)$_2$Hg) and 1/8 and 1 S$_8$. To NMR tubes charged with (**5**-^{t}Bu)$_2$Hg (0.021 g, 1.50×10^{-2} mmol or 0.055 g, 3.94×10^{-2} mmol) and 1 equiv (0.004 g, 1.50×10^{-2} mmol) or 1/8 equiv (0.003 g, 4.93×10^{-3} mmol) of S_8, was distilled C_6D_6 at 77 K. When warmed to 23 °C, the solution became light yellow with a black precipitate, and the analysis showed the formation of **10**-^{t}Bu.

21. [(silox)$_2$Mo=N^{t}Bu]$_2$Hg ((5-^{t}Bu)$_2$Hg) and 1,4,7,10-Tetrathiacyclododecane. To an NMR tube charged with (**5**-^{t}Bu)$_2$Hg (0.035 g, 2.51×10^{-2} mmol) and 1,4,7,10-tetrathiacyclododecane (0.006 g, 3×10^{-2} mmol) was distilled C_6D_6. After two months at 23 °C, a 1:1 mixture of **10**-^{t}Bu and **11**-^{t}Bu formed.

22. [(silox)$_2$Mo=N^{t}Bu]$_2$Hg ((5-^{t}Bu)$_2$Hg) and 1,4,7,10,13,16-Hexathiacyclooctadecane. To an NMR tube charged with (**5**-^{t}Bu)$_2$Hg (0.038 g, 2.72×10^{-2} mmol) and 1,4,7,10,13,16-hexathiacyclooctadecane (0.010 g, 2.7×10^{-2} mmol) was distilled C_6D_6. After 2 months, at 23 °C a 1:1 mixture of of **10**-^{t}Bu and **11**-^{t}Bu formed.

23. (silox)$_2$(O)Mo=N^{t}Bu (9-^{t}Bu) and 1.2 (silox)$_3$Ta. To an NMR tube charged with **9**-^{t}Bu (0.022 g, 3.6×10^{-2} mmol) and 1.2 equiv (silox)$_3$Ta (0.036 g, 4.3×10^{-2} mmol) was distilled in C_6D_6.

24. (silox)$_2$(Cl)Mo=N^{t}Bu (4-^{t}Bu) and 1.05 Ti(N(SiMe$_3$)$_2$)$_3$. To an NMR tube charged with **4**-^{t}Bu (0.026 g, 4.1×10^{-2} mmol) and Ti(N(SiMe$_3$)$_2$)$_3$ (0.022 g, 4.3×10^{-2} mmol) was distilled 0.7 mL benzene-d_6.

25. (silox)$_2$(Cl)Mo=N^{t}Bu (14) and 0.75 Ta(OSi^{t}Bu$_3$)$_3$. To an NMR tube charged with **7**-py (0.021 g, 2.78×10^{-2} mmol) and 2.2 equiv Ta(OSi^{t}Bu$_3$)$_3$ (0.051 g, 6.09×10^{-2} mmol) was distilled in 0.7 mL benzene-d_6.

26. (^{t}Bu$_3$SiO)$_2$(py)$_2$Mo=N^{t}Bu (7-py) and 2.2 Ta(OSi^{t}Bu$_3$)$_3$. To a NMR tube charged with 0.032 g (**5**-^{t}Bu)$_2$Hg was distilled in ~0.7 mL benzene-d_6. When the tube reached 23 °C, analysis showed (silox)$_3$Ta(η^2-N,C-py), but no peaks could be assigned to (^{t}Bu$_3$SiO)$_2$Mo=N^{t}Bu (**5**-^{t}Bu) or degradation products.

27. [(silox)$_2$Mo=N^{t}Bu]$_2$Hg ((5-^{t}Bu)$_2$Hg) thermolysis. To an NMR tube charged with ~10 mg of (**5**-^{t}Bu)$_2$Hg and (**5**-^{t}Amyl)$_2$Hg was added 0.7 mL benzene-d_6. Thermolyses of **8a** at 60 and 100 °C were monitored.

28. [(silox)$_2$Mo=N^{t}Bu]$_2$Hg ((5-^{t}Bu)$_2$Hg) and [(^{t}Bu$_3$SiO)$_2$Mo=N^{t}Amyl]$_2$Hg ((5-^{t}Amyl)$_2$Hg). Benzene-d_6 (0.7 mL) was added to an NMR tube charged with ~10 mg of (**5**-^{t}Bu)$_2$Hg and (**5**-^{t}Amyl)$_2$Hg. The initial analysis at 23 °C indicated only (**5**-^{t}Bu)$_2$Hg and **5**-^{t}Amyl)$_2$Hg, but after 11 h, the reaction mixture was composed of ~25% each of the homotrinuclear compounds and ~50% (**5**-^{t}Bu)Hg(**5**-^{t}Amyl).

NMR Tube Kinetics. General. Sets of three flame-dried NMR tubes, sealed onto 14/20 ground glass joints, were charged with solution of metal reagents (typically ~20 mg, ~1×10^{-5} mol) dissolved in a specific volume of deuterated solvent in the dry box and removed to the vacuum line with a three-prong adaptor. The NMR tubes were degassed and sealed with a torch under active vacuum. Each set of NMR tubes were placed in a temperature-controlled vessel for a measured amount of time, removed, and quickly frozen at 77 K. ^{1}H NMR spectra were taken between every time interval. Alternatively, a tube was placed in the NMR tube in the spectrometer with the probe temperature set to 25 °C, and ^{1}H NMR spectra were taken at specific time intervals, that is, an array experiment. The ^{1}H NMR spectra that were obtained during the monitoring of the crossover of [(silox)$_2$Mo=N^{t}Bu]$_2$Hg ((**5**-^{t}Bu)$_2$Hg) and [(silox)$_2$Mo=N^{t}Amyl]$_2$Hg ((**5**-^{t}Amyl)$_2$Hg) could not be manually integrated because the peaks of the starting materials were too close to those possessed by the crossover product, [(silox)$_2$Mo=N^{t}Bu]Hg[(silox)$_2$Mo=N^{t}Amyl] ((**5**-^{t}Bu)Hg(**5**-^{t}Amyl)). Therefore, to determine the integration values, the spectra had to be deconvoluted using the Varian deconvolution program, which uses Lorentzian lines. When the crossover of (**5**-^{t}Bu)$_2$Hg and (**5**-^{t}Amyl)$_2$Hg) was monitored using an array experiment, the spectra were deconvoluted using a program that individually deconvoluted each ^{1}H NMR spectra using the line-widths and chemical shifts from the statistical mixture of (**5**-^{t}Bu)$_2$Hg, **5**-^{t}Amyl)$_2$Hg and (**5**-^{t}Bu)Hg(**5**-^{t}Amyl) obtained at equilibrium.

29. [(silox)$_2$Mo=N^{t}Bu]$_2$Hg ((5-^{t}Bu)$_2$Hg) Thermolysis. Samples of (**5**-^{t}Bu)$_2$Hg (0.020 g, 1.43×10^{-2} mol) were dissolved in 2 mL benzene-d_6 and monitored at 140 °C to give first-order degradation rate constants of $k = 1.12(4) \times 10^{-4}$, $1.14(3) \times 10^{-4}$, and $1.02(3) \times 10^{-4}$ s^{-1}.

30. [(silox)$_2$Mo=N^{t}Bu]$_2$Hg ((5-^{t}Bu)$_2$Hg) and [(silox)$_2$Mo=N^{t}Amyl]$_2$Hg ((5-^{t}Amyl)$_2$Hg). Varied benzene-d_6 stock solutions of (**5**-^{t}Bu)$_2$Hg and (**5**-^{t}Amyl)$_2$Hg were monitored for crossover.

31. [(silox)$_2$Mo=N^{t}Bu]$_2$Hg ((5-^{t}Bu)$_2$Hg) and [(silox)$_2$Mo=N^{t}Amyl]$_2$Hg ((5-^{t}Amyl)$_2$Hg), Dependence on Hg°. Approximately 0.1 mL of metallic mercury (Hg°) was added to 2.3 mL of benzene-d_6. The solution was shaken vigorously for 20 min, allowed to stand for 12 h, and then shaken vigorously again for 20 min. The mercury was decanted from the benzene-d_6; then 0.010 g of (**5**-^{t}Bu)$_2$Hg (7.16×10^{-3} mmol) and 0.011 g of (**5**-^{t}Amyl)$_2$Hg (7.72×10^{-3} mmol) were dissolved in the a 2 mL volumetric flask using the mercury-saturated benzene-d_6. The solution was transferred into two NMR tubes with a small amount of the previously decanted mercury being added to one tube along with the remaining stock solution. All three were monitored as a group, and the tubes were vigorously shaken between spectra.

Mass Spectrometry. 32. Sample preparation of [(silox)$_2$Mo=N^{t}Bu]$_2$Hg ((5-^{t}Bu)$_2$Hg) and [(silox)$_2$Mo=N^{t}Amyl]$_2$Hg ((5-^{t}Amyl)$_2$Hg) Crossover Mixtures. Equimolar amounts (**5**-^{t}Bu)$_2$Hg and (**5**-^{t}Amyl)$_2$Hg (~0.060 g each) were placed in 4 dram vials, and ~6 mL of benzene was added. The mixtures were stirred for 50 h, or until 20, 50, 65%, or full crossover was revealed by ^{1}H NMR spectroscopy (~10 and ~32 h). The volatiles were then removed in vacuo, and the olive green/brown residue dissolved in ~3 mL of PMe_3. The solution became maroon while warming to

room temperature (RT) and was stirred for 3−5 min, while the solution was warmed from −78 °C to 23 °C. PMe_3 was removed in vacuo; the maroon residue was triturated two times with 4 mL pentane, and the pentane solution was filtered to remove the mercury. Removal of the solvent in vacuo left the crossover mixture of PMe_3 complexes.

33. Preparation of Control Mixtures of PMe_3 Complexes. The PMe_3-ligated complexes were independently synthesized using the procedures described in protocol 7. An equimolar mixture **6**-^{t}Bu and **6**-^{t}Amyl-d_{18} was stirred in pentane for 4 min, followed by the solvent being removed in vacuo. An equimolar mixture of mixture **6**-^{t}Bu, **6**-^{t}Bu-d_{18}, **6**-^{t}Amyl, and **6**-^{t}Amyl-d_{18} was stirred for 4 min, followed by the solvent being removed in vacuo.

34. Mass Spectrum Sample Preparation. The mixtures of PMe_3 complexes (2−3 mg) were dissolved in 1 mL of acetonitrile. The solution was transferred into a vial, which was sealed and taped. The sealed vial was moved to a glove bag near the mass spectrometer. An aliquot of each solution (1 μL) was drawn into a syringe and then injected into the mass spectrometer.

Single-Crystal X-ray Structure Determinations. General. The selected crystal (for 173 K data collection, immersed in polyisobutylene) was placed in the goniometer head of a Siemens SMART CCD area detector system equipped with a fine-focus molybdenum X-ray tube and graphite monochromator. Preliminary diffraction data revealed the crystal system (Table 2), and a hemisphere routine was used to collect the data. Precise lattice constants were determined from a least-squares fit of 15 diffractometer-measured 2θ values. The space group was determined and after correction for Lorentz, polarization, and background effects; unique data were judged observed according to $|F_o| > 2\sigma|F_o|$. Data was processed via the SAINT program. All heavy atoms were located using direct methods (SHELXS and SHELXL), and all non-hydrogen atoms were revealed by successive Fourier syntheses. Full matrix, least-squares refinements (minimization of $\sum w(F_o - F_c)^2$ where w is based on counting statistics modified by an ignorance factor, w^{-1}) with anisotropic heavy atoms, and all hydrogens included at calculated positions led to the final model.

1. (silox)$_2$ClMo=N^{t}Bu (4-^{t}Bu). A purple plate (0.4 × 0.3 × 0.05 mm) from hexanes was used. A total of 21 809 reflections were collected with 10 875 being symmetry independent, and 8979 were judged observed ($R_{int} = 0.0245$). The data was corrected for absorption by SADABS, and the refinement used $w^{-1} = \sigma^2(F_o^2) + (0.0536p)^2 + 0.5839p$, where $p = (F_o^2 + 2F_c^2)/3$). The imido ^{t}Bu-group disorder was modeled with two groups possessing 50% occupancies.

2. [(silox)$_2$Mo=N^{t}Bu]$_2$Hg ((5-^{t}Bu)$_2$Hg). An irregular brown-green block (0.15 × 0.10 × 0.05 mm) from pentane was used. A total of 44 605 reflections were collected with 8812 being symmetry independent and 6712 judged to be observed ($R_{int} = 0.0688$). The data was corrected for absorption by SADABS, and the refinement utilized $w^{-1} = \sigma^2(F_o^2) + (0.0413p)^2 + 3.5939p$, where $p = (F_o^2 + 2F_c^2)/3$). Disorders in the peripheral ^{t}Bu groups were individually modeled using partial occupancies.

3. (silox)$_2$(Me$_3$P)Mo=N^{t}Bu (6-^{t}Bu). A maroon block of (0.4 × 0.35 × 0.25 mm) from pentane was used. A total of 52 242 reflections were collected with 12 000 being symmetry independent and 9825 judged to be observed ($R_{int} = 0.0374$). The data was corrected for absorption by SADABS, and the refinement used $w^{-1} = \sigma^2(F_o^2) + (0.0488p)^2 + 6.4878p$, where $p = (F_o^2 + 2F_c^2)/3$).

4. (silox)$_2$(4-pic)$_2$Mo=N^{t}Bu (7-4-pic). A blue-purple block (0.3 × 0.25 × 0.05 mm) from hexanes was used. A total of 46 216 reflections were collected with 9351 being symmetry independent and 7883 judged to be observed ($R_{int} = 0.0769$). The data was corrected for absorption by SADABS, and the refinement used $w^{-1} = \sigma^2(F_o^2) + (0.0648p)^2 + 42.6282p$, where $p = (F_o^2 + 2F_c^2)/3$). The poor data quality may have been a result of twinning.

Acknowledgment. P.T.W. would like to thank the National Science Foundation (CHE-0415506) and Cornell University for financial support. T.R.C. thanks the National Science Foundation (CHE-0309811) and the Department of Energy (DEFG02-03ER15387) for support of this research. We would also like to thank Prof. Karsten Meyer (UCSD and University of Erlangen-Nuremberg) for data collection (SQUID) and Profs. Francis J. DiSalvo and Barry K. Carpenter for helpful discussions.

Supporting Information Available: CIF files for **4**-^{t}Bu, **6**-^{t}Bu and **7**-4-pic. The CIF file for (**5**-^{t}Bu)$_2$Hg and computational details including a bibliography can be found in the Supporting Information for ref 19. This material is available free of charge via the Internet at http://pubs.acs.org.

IC7010953